

Máster en Ingeniería de Sistemas y Control

Simulación de control de formaciones de satélites utilizando propulsión eléctrica

Simulation of a control system for electric propulsion satellite formations

Autor: Ricardo Manuel Navarro Vásquez
Director: Segundo Esteban San Román

Curso 2017-2018. Convocatoria de Septiembre



Máster en Ingeniería de Sistemas y Control

Simulación de control de formaciones de satélites utilizando propulsión eléctrica

Simulation of a control system for electric propulsion satellite formations

Autor: Ricardo Manuel Navarro Vásquez
Director: Segundo Esteban San Román

2018

Autorización

Autorizamos a la Universidad Complutense y a la UNED a difundir y utilizar con fines académicos, no comerciales y mencionando expresamente a sus autores, tanto la memoria de este Trabajo Fin de Máster, como el código, la documentación y/o el prototipo desarrollado.

Firmado: Ricardo Manuel Navarro Vásquez



Firma del alumno

Abstract

This project aims to perform a preliminary dimensioning to model a control system for CubeSats in formation flying to evaluate the implementation of micro-electric propulsion. An overall assessment has been performed of nanosatellites, micro-electric propulsion, formation flying, control strategies and their current trends. A mission with a platform has been proposed in order to have a set of design constraints that guide the development process. A theoretical model of orbital dynamics and relative motion has been presented, from which a plant and a control system have been developed. A dynamics, kinetics an environment model has been implemented in order to compare its results with the ones obtained from the plant. Simulation test results are presented and discussed. Finally, a proposal for future works is made.

Keywords: CubeSat, formation flying, electric propulsion, control, error-space, state-space, DKE.

Acknowledgments

In Spanish. Me es difícil escribir un texto de agradecimiento cuando son tantas las personas, tanta la ayuda que me han mostrado, que unas pocas palabras no parecen ser reconocimiento suficiente. Ha sido complejo sortear las muchas dificultades —y la limitada capacidad que se tiene con un niño pequeño—, pero al escuchar palabras como «*no te preocupes, tu estudia, que ya me encargo yo*» se siente el cariño y la fuerza de una gran familia y de unos grandes amigos.

A todos, sinceramente, gracias.

Contents

1 Introduction **1**
1.1 Motivation and Scope . . . 1
1.2 State of the art . . . 1
1.2.1 Nanosatellites . . . 1
1.2.2 Formation Flying . . . 2
1.2.3 Micro-electric propulsion . . . 3
1.2.4 Control . . . 5
1.3 Tools and configuration . . . 6

2 Mission and Platform **7**
2.1 Mission description . . . 7
2.2 Platform description . . . 8
2.3 Other mission parameters . . . 9

3 Theoretical model **10**
3.1 Plant and environment modeling . . . 10
3.1.1 Coordinate systems . . . 10
3.1.1.1 Earth Centered Inertial — ECI . . . 10
3.1.1.2 Keplerian Elements . . . 11
3.1.1.3 Satellite frame — RSW . . . 16
3.1.2 Dynamics, Kinetics and Environment . . . 20
3.1.3 Hill-Clohessy-Wiltshire equations . . . 23
3.2 Control system modeling . . . 24
3.3 Integrated system . . . 31
3.3.1 Case 1: Proposed nominal case . . . 32
3.3.2 Case 2: Alternative case . . . 35

4 Simulations and results **38**
4.1 Test cases . . . 39
4.2 Test results . . . 40

4.2.1 No sensor error 40
4.2.1.1 Case 1 40
4.2.1.2 Case 2 42
4.2.2 With sensor error 45

5 Results discussion and future work **50**
5.0.1 Future work 50

A Glossary of symbols **52**

B Glossary of acronyms **56**

C Annex — List of Matlab™ and Simulink™ files **57**

Bibliography **58**

List of Figures

1.1 Proba-3 formation — *occulter* spacecraft shadowing the Sun for *coronograph* spacecraft 3

3.1 ECI coordinate system and satellite orbit 11
3.2 Example of Keplerian Elements for a generic circular orbit 12
3.3 Position and velocity in ECI to Keplerian elements 14
3.4 Argument of latitude calculation 15
3.5 Right ascension of ascending node calculation 15
3.6 Inclination calculation 15
3.7 Keplerian elements to position and velocity in ECI 15
3.8 Conversion from Keplerian elements to orbital-plane position 16
3.9 Conversion from Keplerian elements to orbital-plane velocity 16
3.10 RSW coordinate system in ECI frame 17
3.11 Orbit precession in ECI frame 18
3.12 Overview of the DKE Simulink™ model 22
3.13 Model of the two-body acceleration 22
3.14 J2 zonal harmonic model 22
3.15 Atmospheric drag model 22
3.16 Atmospheric density model 23
3.17 Leader satellite model 23
3.18 State-Space model of the plant 26
3.19 Control model using error-space 29
3.20 Simulink™ model for parameter tuning 32
3.21 Case 1 — Position response in S axis 33
3.22 Case 1 — Position response in RW axes 33
3.23 Case 1 — Error response 34
3.24 Case 1 — Thrust response 34
3.25 Case 2 — Position response in S axis 35
3.26 Case 2 — Position response in RW axes 36
3.27 Case 2 — Error response 36
3.28 Case 2 — Thrust response 37

4.1 Complete simulation model 38
4.2 Integrated DKE used for the simulations 38
4.3 Model used to check the distance when the satellites are left uncontrolled 39
4.4 Uncontrolled distance between leader and follower satellites 39
4.5 Case 1: Simulation without sensor error — Position in S axis 41
4.6 Case 1: Simulation without sensor error — Position in RW axes 41
4.7 Case:1 Simulation without sensor error — Error response 42
4.8 Case 1: Simulation without sensor error — Thrust demand 43
4.9 Case 2: Simulation without sensor error — Position in S axis 43
4.10 Case 2: Simulation without sensor error — Position in RW axes 44
4.11 Case:2 Simulation without sensor error — Error response 44
4.12 Case 2: Simulation without sensor error — Thrust demand 45
4.13 Case 2: Simulation with sensor error — Perturbed and perceived positions in R axis 46
4.14 Case 2: Simulation with sensor error — Perturbed and perceived positions in S axis 46
4.15 Case 2: Simulation with sensor error — Perturbed and perceived positions in W axis 47
4.16 Case 2: Simulation with sensor error — Actual position in S axis 47
4.17 Case 2: Simulation with sensor error — Actual position in RW axis 48
4.18 Case 2: Simulation with sensor error — Error 48
4.19 Case 2: Simulation with sensor error — Detail of 1000 s of thrust in steady-state . . 49

List of Tables

1.1 Potential micro-electric propulsion systems for proposed mission. 4

1 Introduction

1.1 Motivation and Scope

This project aims to perform a preliminary dimensioning to model a control system for CubeSats in formation flying. In order to achieve this goal it will be necessary to model several systems like the plant; dynamics, kinetics and environment (or DKE); control; and coordinate systems with their corresponding transformations.

CubeSats are a relatively new space platform, with a mass range of about 1 kg to 12 kg for the most used types, that is accessible to educational institutions or small companies that do not have the funding for traditional satellite developments. With this platform, these entities are now considering formation flying missions, which can provide better performances than traditional single-satellite missions.[1]

The electric propulsion is a technology that provides low thrust but high specific impulse and can be very useful for compensating drag and other perturbations. However, their low thrust might impose significant restrictions on the capacity of formation maintenance.[2] Therefore, it is necessary to analyze each mission and its thrust demands in order to ensure that electric propulsion is viable in such scenarios.

1.2 State of the art

1.2.1 Nanosatellites

Nanosatellites are artificial satellites with a wet mass between 1 kg to 12 kg. Among them, the CubeSat[3] standard is perhaps the most extended one. In this way, current nanosatellites are usually constituted by several CubeSat $10\,\mathrm{cm}^3 \times 10\,\mathrm{cm}^3 \times 10\,\mathrm{cm}^3$ (U) having a mass of no more than 1.33 kg per unit. There are single-unit (1U), two-unit (2U), three-unit (3U) and up to six-unit (6U)[4] CubeSats that lay within the nano-satellite definition range, with recent developments

[1] Manuel Angulo Jerez et al., "Control de Formaciones en Vuelo de Satélites de Bajo Coste," Creative Commons Attribution CC-BY-NC 3.0 license, 2018, https://creativecommons.org/licenses/by-nc/3.0/.

[2] Eviatar Edlerman and Igal Kronhaus, "Analysis of Nanosatellite Formation Establishment and Maintenance Using Electric Propulsion," *Journal of Spacecraft and Rockets* 54, no. 3 (May 2017): 731–742, ISSN: 0022-4650, doi:10.2514/1.a33632, https://doi.org/10.2514/1.A33632.

[3] http://www.cubesat.org/about/

[4] California Polytechnic State University, *6U CubeSat Design Specification*, technical report (California Polytechnic State University, April 20, 2016).

leading towards bigger 12U and 24U sizes.

These systems often use commercial off-the-shelf (COTS) components for their electronics and structure. In this way, the nanosatellites are allowing to put in orbit relatively low-cost systems to accomplish different kind of missions such as: technology demonstration, Earth observation, science, etc. For 3U CubeSats and larger, the spacecraft can even include thrusters and reaction wheels in addition to the solar panels, batteries, telemetry and command and control systems that may be found on such satellites. This enhances the capability of such platforms for different actuation schemes, enabling complex missions, such as formation flying, based on small and low-cost systems.

1.2.2 Formation Flying

The availability of small, cheap, and capable spacecraft, coupled with the fact the launchers often carry multiple CubeSats for deployment, presents the opportunity to fly pairs or triplets of satellites in formation, which may be beneficial in some applications.

Multisatellite missions can be broadly divided into two categories:

- Formation Flying (FF) missions.
- Constellation missions.

The formation maintenance requires the capability to control the absolute and relative positions of the spacecrafts in the formation within a certain distance while maintaining a specific level of accuracy in such distance knowledge and control. This controllability and precision requirements, together with the relatively small inter-satellite distances in the formation (from meters to a few kilometers), is the difference with respect to satellites constellations, that rely only on its own position and velocity.

In addition to this, the dynamic states of formation flying satellites are coupled through a common control law. In other words, in an FF mission, at least one satellite must track a desired state relative to another satellite, and its tracking control law must, at the minimum, depend upon the states of this satellite.[5]

Formation Flying techniques and associated technologies have already been proved in several Space missions worldwide. PRISMA[6] is a Swedish-led mission that was launched in 2010 with the objective to develop and qualify new technology necessary for future formation flying missions. Currently, within a Spanish-led consortium, ESA is developing PROBA-3[7], a system consisting of two spacecrafts flying in very precise formation that will be launched in 2020. PROBA-3 will implement very precise sensors and innovative control algorithms to probe the capabilities of such

[5] Saptarshi Bandyopadhyay et al., "Review of Formation Flying and Constellation Missions Using Nanosatellites," *Journal of Spacecraft and Rockets* 53, no. 3 (2016): 567–578, doi:10.2514/1.a33291.

[6] Staffan Persson, Simone D'Amico, and Jon Harr, "Flight Results from PRISMA Formation Flying and Rendezvous Demonstration Mission," *61st International Astronautical Congress 2010, IAC 2010*, 2010,

[7] http://www.aeroespacial.sener/productos/proba-3

systems to maintain very accurate virtual structures enabling new science missions (e.g. XEUS, LISA).

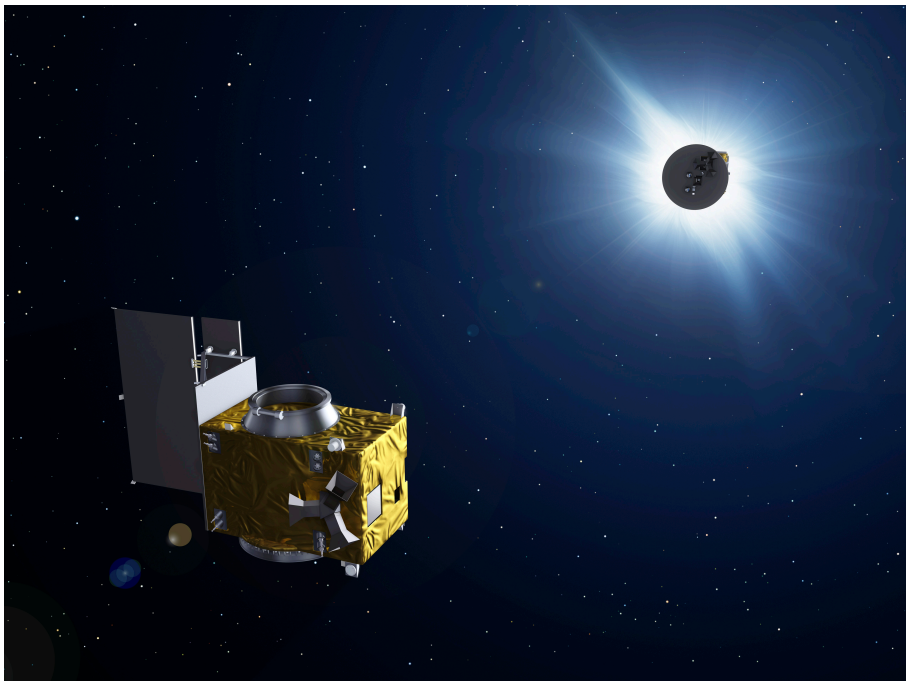


Figure 1.1: Proba-3 formation — *occulter* spacecraft shadowing the Sun for *coronograph* spacecraft
From: European Space Agency, 2013

These two examples are formation flying systems based on small satellites (<180 kg). In the mass range of 1 kg to 12 kg, CubeSats have strict constraints on allowed mass, volume, and electrical power and they are equipped with only limited sensor and actuator capabilities.

However, formation flying systems implemented on nanosatellites can still be realizable with current state-of-the-art technology and provide important results for Science, Earth Observation and technology demonstration missions. This last application is the one more extended nowadays among the nanosatellites based formation flying missions that are under development worldwide.[8]

1.2.3 Micro-electric propulsion

The main challenges of FF missions stem from dynamic couplings between satellites and the environment. In order to maintain a precise satellite formation over a long period of time, the satellites need to mitigate the drifts created by the initial orbit injection, the effects the in-orbit perturbations have on the implied platforms and any other disturbances that may affect the formation shape and size. This is achievable only with the help of propulsion devices that can control the position of the satellites.

Spacecraft propulsion systems can be divided into chemical propulsion systems of electric propulsion systems. While chemical propulsion systems store their energy in the propellants, the energy required by electric propulsion systems is generated by solar panels.

[8] Bandyopadhyay et al., "Review of Formation Flying and Constellation Missions Using Nanosatellites."

In chemical propulsion the achievable exhaust velocity (or specific impulse) is limited by the reactants fixed amount of energy per unit mass. However, because the propellants are their own energy source, very high powers and thrust levels can be achieved.

An arbitrarily large amount of energy can be delivered to a given mass of propellant in an electric propulsion thruster, so that the exhaust velocity (or specific impulse) can be much larger than that available from a chemical propulsion system. However, the rate at which energy from the external source is supplied to the propellant is limited by the mass available for the power system. This limits the thrust of the electric propulsion system for a given spacecraft mass. Because of this, electric propulsion devices tend to be low thrust to mass ratio (and therefore low acceleration) thrusters.

Although electric propulsion equipped vehicles have low thrust to mass ratios, they can have a larger total amount of impulse than a chemical propulsion system. Moreover, electric propulsion devices provide better thrust level controllability in the micro-Newtons thrust level[9]. It is also to be noted, that there are very few chemical propulsion engines providing thrust below the milli-Newton range, and these thrusters (cold gas thrusters) are very low performers in terms of propellant mass consumption. These facts make micro-electric propulsion thrusters very good candidates for nanosatellites formation flying missions if the required power levels can be ensured.

The table 1.1 compiles performance information related to currently flight ready (or even flight-proven) electric propulsion thrusters that can serve the purpose of the mission discussed in the present work.

Thruster designation	Thruster type	Manufacturer	Power [W]	Thrust [µN]	Specific Impulse [s]	Total impulse [N s]
IFM Nano Thruster [a]	Field Emission Electric Propulsion	Enpulsion	35	<500	2000-5000	>5000
BET-1mN [b]	Electrospray	Busek	15	<700	400-1300	605
RIT-mX[c]	Radiofrequency Ion Thruster	Arianegroup	50	<500	300-3000	>3500
Microresistojet [d]	Resistojet	Busek	15	10000	150	404
Neptune [e]	Neutralizer-Free Gridded Ion Thruster	Thrustme	60	<700	1000	

[a] https://www.enpulsion.com/
[b] http://www.busek.com/
[c] http://www.space-propulsion.com/
[d] http://www.busek.com/
[e] http://thrustme.fr/

Table 1.1: Potential micro-electric propulsion systems for proposed mission.

[9] http://sci.esa.int/smart-1/34201-electric-spacecraft-propulsion/?fbodylongid=1534

1.2.4 Control

Regarding the control strategies that can be used, a paper from Kristiansen and Nicklasson[10] lists and discusses several alternatives, e.g. PD, Linear-Quadratic, Lyapunov-based, etc. However, in Franklin, Powell, and Emami-Naeini[11] an error-space approach based on the state-space equations of the plant is presented. This type of control aims to follow a reference input profile with no steady-state error and with disturbance rejection capabilities. In the present project a simplified version is used.

For modeling the relative motion of the satellites there are some alternatives, based on the linearity of the equations, assumptions and types of orbit:[12] Clohessy-Wiltshire equations, Lawden equations, Tschauner–Hempel equations, Manikonda et al. etc. However, according to Angulo Jerez et al.,[13] it is possible to use the Clohessy-Wiltshire equations to model the relative motion of two CubeSats in formation flying, and in addition analyze the energy requirements for each potential case. However, this set of equations have two distinctive characteristics that would need to be taken into account:[14]

- They do not contain orbit perturbation contributions, e.g. J2 Zonal Harmonic or atmospheric drag.
- They are a set of linearized differential equations that can be used to create control systems in Simulink™, and take into account relative motion in non-inertial frames.

A low energy configuration that can be used as a first approach would be an along-track formation, in which there are a leader and a follower satellite, both in the same orbit, with the follower lagging behind some meters after the leader.[15] There are other configurations that can be used, depending on the mission; however, for this project, an along-track formation is going to be considered.

It would be possible to use a DKE to simulate the thrust requirements for the scenarios and control systems proposed in Angulo Jerez et al.[16] and assess the effects of added perturbations like J2 Zonal Harmonic or atmospheric drag.

There is a last consideration that should be taken into account, when the thrusters are oriented in order to keep the formation, the satellite's orientation may not be appropriate for payload operation. Therefore, it would be necessary to assign time slots for operations and time slots to

[10] Raymond Kristiansen and Per Johan Nicklasson, "Spacecraft formation flying: A review and new results on state feedback control," *Acta Astronautica* 65, nos. 11-12 (2009): 1537–1552, doi:10.1016/j.actaastro.2009.04.014.

[11] Gene F. Franklin, J. David Powell, and Abbas Emami-Naeini, *Feedback Control of Dynamic Systems, 4th Edition* (Prentice Hall, 2002), ISBN: 0130323934.

[12] Kristiansen and Nicklasson, "Spacecraft formation flying: A review and new results on state feedback control."

[13] Angulo Jerez et al., "Control de Formaciones en Vuelo de Satélites de Bajo Coste."

[14] Ibid.

[15] Ibid.

[16] Ibid.

keep the formation. There are different strategies[17] that can be implemented that are oriented to keep fuel consumption low, e.g. static time slots, dynamic time slots, cosine methods, etc. These are not being considered for the present project, however, they would be important for an attitude control system definition.

1.3 Tools and configuration

In this project the tools used are:

- MathWorks, Inc. Matlab™ 2018a Student Version and its toolboxes
- MathWorks, Inc. Simulink™ 2018a Student Version and its blocksets
- macOS 10.13.6
- MacTeX 2018
- MacHg 1.0.2 with Mercurial 2.0 for configuration control.

As most of the contents are analyses and simulations, there are no specific requirements besides a typical PC with Matlab™/Simulink™ and access to relevant literature.

[17] Edlerman and Kronhaus, "Analysis of Nanosatellite Formation Establishment and Maintenance Using Electric Propulsion."

2 Mission and Platform

2.1 Mission description

Before proceeding to the technical aspects of the design of a control system, it is necessary to identify the type of missions, platforms and overall requirements, for which the control can be considered valid.

In this context, the mission analysis provides the set of requirements that will serve as the base to generate the complete satellite design. This analysis is comprised by several activities[1] which include —but ar not limited to— e.g. orbit and constellation design, space environment, payload design, spacecraft and subsystems design, manufacturing, propulsion, etc. In this project, a concrete set of mission parameters has been selected as they have been considered representative enough of potential use scenarios.

Institutions, universities and small companies can consider small CubeSat formations because they can offer a possibility to implement functionalities usually reserved for large single mission satellites, such as low cost synthetic aperture radars,[2] large interferometers,[3] earth observation, etc.

Therefore the following scenario is proposed,

Low Earth Orbit This kind of orbit is a good candidate for these type of missions as the distance to the Earth is shorter and improves the resolution of the payload;[4] in addition, sun-synchronous orbits can be used. In the present project an altitude of 450 km over the Earth is proposed.

Sun-synchronous A dawn-dusk sun-synchronous orbit[5] has a precession such that it maintains an approximately equal orientation with respect to the sun throughout the year, following the dawn-dusk line. Among its benefits, the satellite has constant sun available for electric

[1] J. R. Wertz and W. J. Larson, *Space Mission Analysis and Design, 3rd edition (Space Technology Library, Vol. 8)* (Microcosm, 1999), ISBN: 1881883108.

[2] E. H. Peterson, G. Fotopoulos, and R. E. Zee, "A Feasibility Assessment for Low-Cost InSAR Formation-Flying Microsatellites," *IEEE Transactions on Geoscience and Remote Sensing* 47, no. 8 (2009): 2847–2858, doi:10.1109/tgrs.2009.2017521.

[3] Alessandro Ferrario and Beatrice Furlan, "CubeSat formation flying mission as Wi-Fi data transmission and GPS based relative navigation technology demonstrator" (master's thesis, Politecnico di Milano, 2011).

[4] Wertz and Larson, *Space Mission Analysis and Design, 3rd edition (Space Technology Library, Vol. 8)*.

[5] Ibid.

power generation, and any image of the ground has approximately the same illumination, which facilitates the work of imaging based payloads. These kind of orbits are available at the altitude proposed above and for this case is retrograde with an inclination of 97.21 deg.

Leader-follower configuration As discussed in §1.2.4, this low energy configuration can be used as a first approach for the dimensioning of the formation.

Inter-satellite distance Although the distance between the two satellites has to be defined based on particular missions, an starting point of 200 m has been selected as it seems to provide an adequate trade-off between thruster demand and formation size, and it is well within the outdoor range of several commercial Wi-Fi devices,[6] which is around 200 m to 2800 m, with some units reaching even farther. On the other hand, for the distance measurement, GPS sensors would be a very good option in these kind of orbits as the GPS the service is available (the satellites are in a much higher orbit).

Micro-electric propulsion The advantages of using electric propulsion in CubeSats have been presented in §1.2. For this project it is proposed to stay well below 1 mN in order to stay within the limits of the commercial thrusters assessed in Table 1.1.

2.2 Platform description

The CubeSat platform has been standardized by the California Polytechnic State University in or order to lower the cost of implementation.[7] By reusing the same design and procuring commercial-off-the-shelf (COTS) parts, the manufacturing costs of the subsystems are reduced, the development time shortens and the entry barrier lowers.

This platform, in the 6U size,[8] is a type of nano-satellite that can be contained in a fully standardized Canisterized Satellite Dispenser[9] and deployed when reaching the desired orbit, they are big enough to accommodate some micro-electrical propulsion devices with GPS sensor and are adequate for low cost missions.

Some 6U solar panels can produce about 17 W of electrical power[10], therefore, in order to accommodate some micro-electric propulsion devices without consuming all the power, it would be necessary to deploy several panels. As the power obtained from solar panels depend on the surface, it might be necessary to consider larger CubeSat sizes for some missions (e.g. 12U or even 24U).

[6] Ferrario and Furlan, "CubeSat formation flying mission as Wi-Fi data transmission and GPS based relative navigation technology demonstrator."

[7] Ibid.

[8] California Polytechnic State University, *6U CubeSat Design Specification*.

[9] Planetary Systems Corporation, *Payload Specification for 3U, 6U, 12U and 27U*, technical report (Planetary Systems Corporation, July 21, 2014).

[10] From ISIS - Innovative Solutions in Space: `https://www.isispace.nl/product/isis-cubesat-solar-panels/`

2.3 Other mission parameters

The following conditions have been derived from the mission and platform descriptions and will be used throughout the project,

- Coefficient of drag: 2.2.[11]
- Mass of the CubeSat: 12 kg.[12]
- CubeSat height: 100×10^{-3} m.[13]
- CubeSat width: 226.3×10^{-3} m.[14]
- CubeSat length: 366×10^{-3} m.[15]
- Epoch: 2000-03-20, 07h 35m 00s.
- Satellite altitude: 4.5×10^{5} m.
- Orbit inclination: 97.21 deg.
- Distance between leader and follower: 200 m behind the follower.

[11] Wertz and Larson, *Space Mission Analysis and Design, 3rd edition (Space Technology Library, Vol. 8)*.
[12] Planetary Systems Corporation, *Payload Specification for 3U, 6U, 12U and 27U*.
[13] California Polytechnic State University, *6U CubeSat Design Specification*.
[14] Ibid.
[15] Ibid.

3 Theoretical model

3.1 Plant and environment modeling

In order to define the control and the simulation environment it is necessary to establish first a model of the Dynamics, Kinetics and Environment, hereafter DKE.

It is perhaps the works of Johannes Kepler and Sir Isaac Newton the ones that provided the means to perform precise quantitative analyses of the kinematics and dynamics of planetary motion, respectively. As satellite orbits are subject to these same principles, the theoretical models have been based on Kepler's laws and Newton's two-body equations of motion for the special case of LEO circular orbits around earth.

Before starting any consideration it would be necessary to define some coordinate systems.

3.1.1 Coordinate systems

3.1.1.1 Earth Centered Inertial — ECI

A fully inertial reference frame is difficult to obtain and would impose complex calculations that would not add significant benefits to the model; however, a quasi-inertial[1] frame can be considered inertial for this application. For this project, an Earth Centered Inertial[2] frame —or ECI— is sufficient and ensures that Newton's equations of motion are still valid. The ECI in this particular case is defined as follows:

- The $\hat{i}$ axis points towards the vernal equinox of year 2000.
- The $\hat{j}$ axis together with $\hat{i}$ form a plane contained in the equatorial plane.
- The $\hat{k}$ axis points toward the north pole in order to form an orthonormal frame.

This coordinate system maintains the orientation as time passes and it is not fixed to the earth's rotation. Satellite orbits describe a circle centered in the origin of the ECI coordinate system. Figure 3.1 depicts the satellite orbit and the ECI frame.

[1] David A. Vallado, *Fundamentals of Astrodynamics and Applications, 4th ed. (Space Technology Library)* (Microcosm Press, 2013), ISBN: 9781881883180.

[2] Ibid.

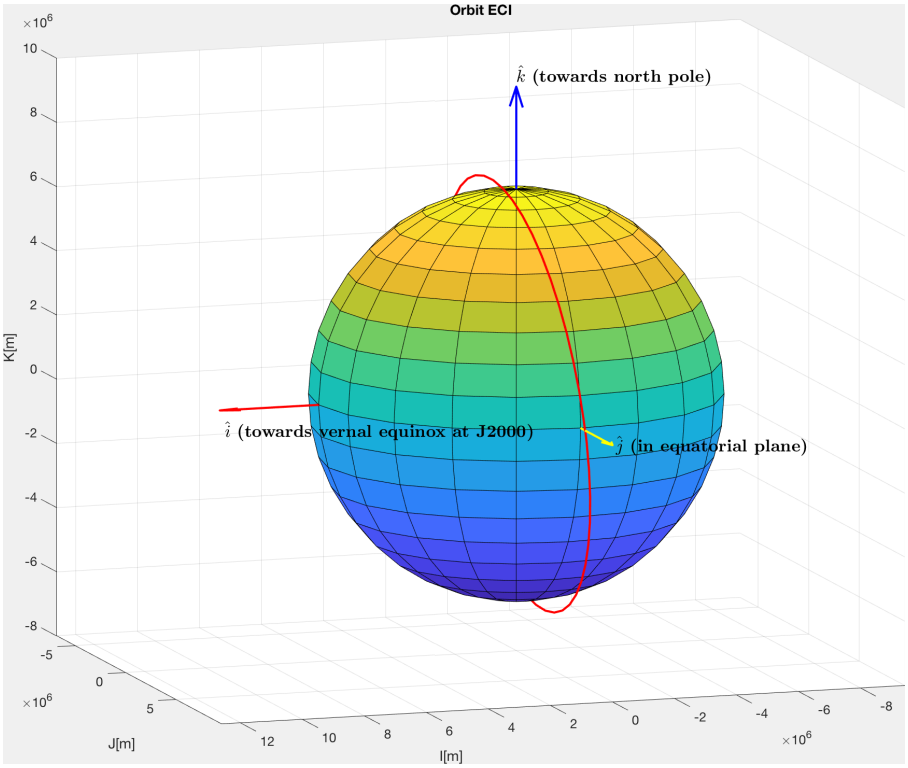


Figure 3.1: ECI coordinate system and satellite orbit

3.1.1.2 Keplerian Elements

Although position, velocity and acceleration vectors can be referenced in this frame, it is often more convenient to use classical orbital parameters to describe orbits and the position of the satellites in it. In addition, several of these parameters serve also to define some orbital parameters throughout the project. These classical orbital parameters, also known as Keplerian elements, can describe any orbit, and in the case of circular ones they offer some simplifications. The classical orbital parameters are:[3]

Semi-major axis (a) In the case of circular orbits, the Perigee, Apogee, Semi-parameter, and Semi-major axis are all equal to the **radius of the orbit**, which is unique.

Eccentricity (e) In the case of circular orbits it is equal to zero.

Inclination (i) Is the angle between the $\hat{k}$ vector and the angular momentum vector $\vec{\mathbf{h}}$ which defines the orbit plane.

Right ascension of the ascending node (Ω) It is the angle from the $\hat{i}$ vector to the point in the equator plane were the satellite crosses from south to north, i.e. the **ascending node**. It is measured in the $\hat{i}\hat{j}$ plane counterclockwise from $\hat{i}$.

[3] Vallado, *Fundamentals of Astrodynamics and Applications, 4th ed. (Space Technology Library)*.

Argument of the perigee (ω) As there is no perigee in circular orbits, this parameter is not defined.

True anomaly (ν) As there is no perigee/periapsis in circular orbits, this parameter is substituted by the **argument of latitude** (u); which is the angle measured between the ascending node and the position vector of the orbiting body.

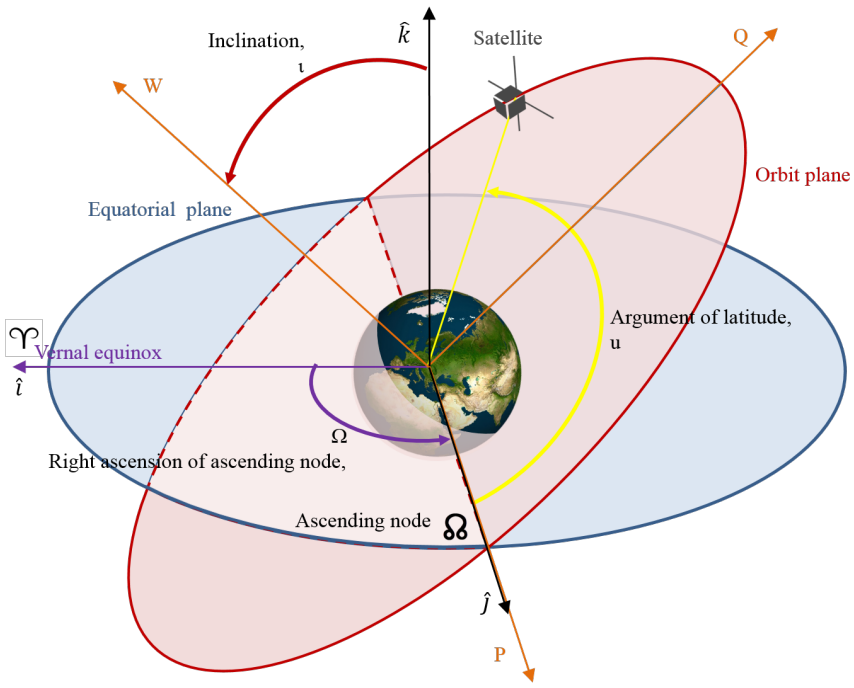


Figure 3.2: Example of Keplerian Elements for a generic circular orbit

It is possible to transform position and velocity from ECI to Keplerian elements. The method[4] described below is specific for circular orbits.

First it is necessary to obtain the angular momentum $\vec{\mathbf{h}}$.

$$\vec{\mathbf{h}}_{eci} = \vec{\mathbf{r}}_{eci} \times \vec{\mathbf{v}}_{eci} \tag{3.1}$$

Where $\vec{\mathbf{r}}_{eci} \times \vec{\mathbf{v}}_{eci}$ are the position and velocity vectors of the satellite in the ECI coordinate frame.

The vector pointing to the ascending node will determine the reference from which the position of the satellite is determined,

$$\vec{\mathbf{n}} = \hat{k} \times \vec{\mathbf{h}}_{eci} \tag{3.2}$$

The argument of latitude can then be calculated,

[4]Vallado, *Fundamentals of Astrodynamics and Applications, 4th ed. (Space Technology Library)*.

$$u = \begin{cases} \operatorname{acos}\left(\frac{\vec{\mathbf{n}}\cdot\vec{\mathbf{r}}_{eci}}{\|\vec{\mathbf{n}}\|\|\vec{\mathbf{r}}_{eci}\|}\right) & r_{k_{eci}} \geq 0 \\ 2\pi - \operatorname{acos}\left(\frac{\vec{\mathbf{n}}\cdot\vec{\mathbf{r}}_{eci}}{\|\vec{\mathbf{n}}\|\|\vec{\mathbf{r}}_{eci}\|}\right) & r_{k_{eci}} < 0 \end{cases} \tag{3.3}$$

The right ascension of the ascending node can then be calculated as follows,

$$\Omega = \begin{cases} \operatorname{acos}\left(\frac{n_i}{\|\vec{\mathbf{n}}\|}\right) & n_j \geq 0 \\ 2\pi - \operatorname{acos}\left(\frac{n_i}{\|\vec{\mathbf{n}}\|}\right) & n_j < 0 \end{cases} \tag{3.4}$$

The inclination can be calculated as follows,

$$i = \frac{h_k}{\left\|\vec{\mathbf{h}}_{eci}\right\|} \tag{3.5}$$

The last element, the radius of the orbit, is the norm of the position vector,

$$a = \|\vec{\mathbf{r}}_{eci}\| \tag{3.6}$$

It is also possible to perform the inverse transformation, from Keplerian elements to ECI, however it is necessary to introduce first the perifocal coordinate frame,[5] or PQW, which is also a quasi-inertial frame.

In this frame, the satellite motion is contained in the PQ plane, and the W axis is perpendicular to form an orthonormal frame. The P axis points towards the perigee, however, as it is not defined for circular orbits, the following convention is used: $\omega = 0$, i.e. the origin of the argument of latitude is contained in the equator plane $\hat{i}\hat{j}$.

The method[6] below uses the perifocal coordinate frame to transform from Keplerian elements to ECI.

First it is necessary to calculate the position and velocity vectors in the perifocal plane,

$$\vec{\mathbf{r}}_{pqw} = \begin{pmatrix} a\cos(u) \\ a\sin(u) \\ 0 \end{pmatrix} \tag{3.7}$$

$$\vec{\mathbf{v}}_{pqw} = \begin{pmatrix} -\sqrt{\frac{\mu}{a}}\sin(u) \\ \sqrt{\frac{\mu}{a}}\cos(u) \\ 0 \end{pmatrix} \tag{3.8}$$

where a is the radius of the orbit, u is the argument of latitude and μ is the gravitational parameter:

$$\mu = Gm_{\oplus} \tag{3.9}$$

[5] Vallado, *Fundamentals of Astrodynamics and Applications, 4th ed. (Space Technology Library)*.
[6] Ibid.

Where G is the universal gravitational constant and $m_{\oplus}$ is the mass of the Earth. Note that as the mass of the satellite is negligible compared to the mass of the Earth it is not present in the formula.

These position and velocity vectors are then transformed from PQW to ECI by means of a rotation matrix $\mathbf{M}_{pqw}^{ijk}$,

$$\begin{cases} \vec{\mathbf{r}}_{eci} = \mathbf{M}_{pqw}^{eci} \cdot \vec{\mathbf{r}}_{pqw} \\ \vec{\mathbf{v}}_{eci} = \mathbf{M}_{pqw}^{eci} \cdot \vec{\mathbf{v}}_{pqw} \end{cases} \tag{3.10}$$

where,

$$\mathbf{M}_{pqw}^{eci} = \begin{pmatrix} \cos(\Omega) & -\cos(i)\sin(\Omega) & \sin(i)\sin(\Omega) \\ \sin(\Omega) & \cos(i)\cos(\Omega) & -\cos(\Omega)\sin(i) \\ 0 & \sin(i) & \cos(i) \end{pmatrix} \tag{3.11}$$

A Simulink™ model has been created in order to convert from ECI position and velocity to Keplerian elements. The overview of the model is in Figure 3.3, and the different calculations in Figure 3.4, Figure 3.5 and Figure 3.6.

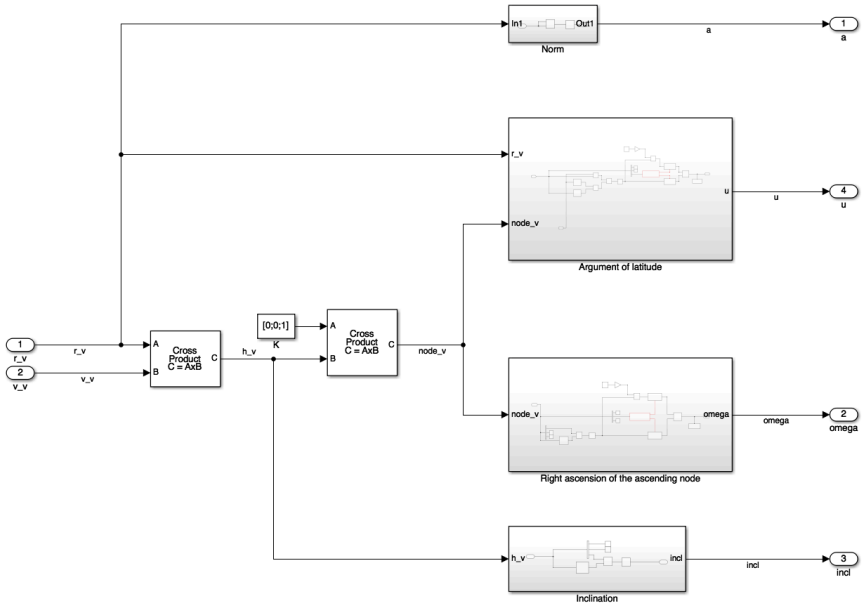


Figure 3.3: Position and velocity in ECI to Keplerian elements

The inverse calculation, from Keplerian elements to ECI position and velocity can be seen in Figure 3.7. The sub-blocks necessary to calculate orbital-plane position and velocity are depicted in Figure 3.8 and Figure 3.9.

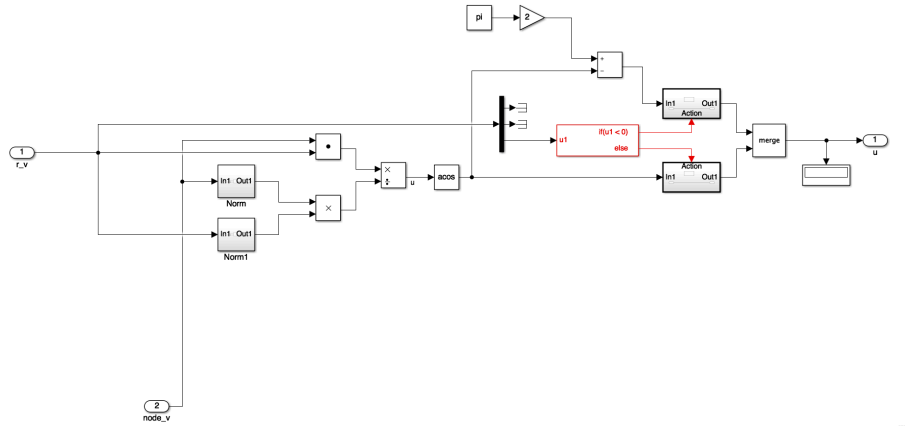


Figure 3.4: Argument of latitude calculation

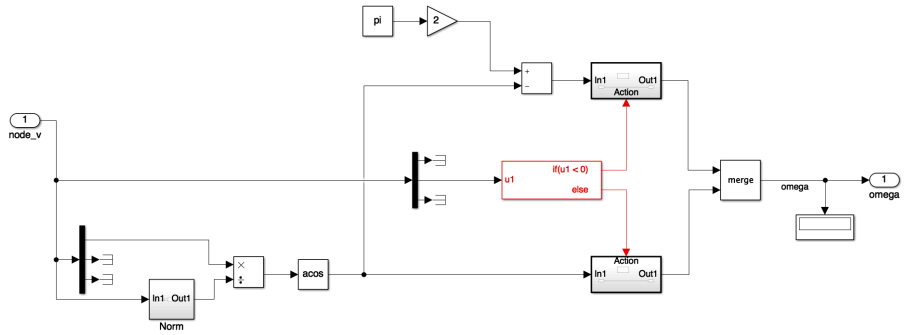


Figure 3.5: Right ascension of ascending node calculation

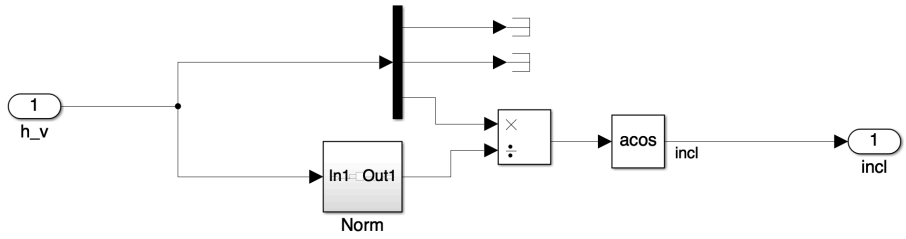


Figure 3.6: Inclination calculation

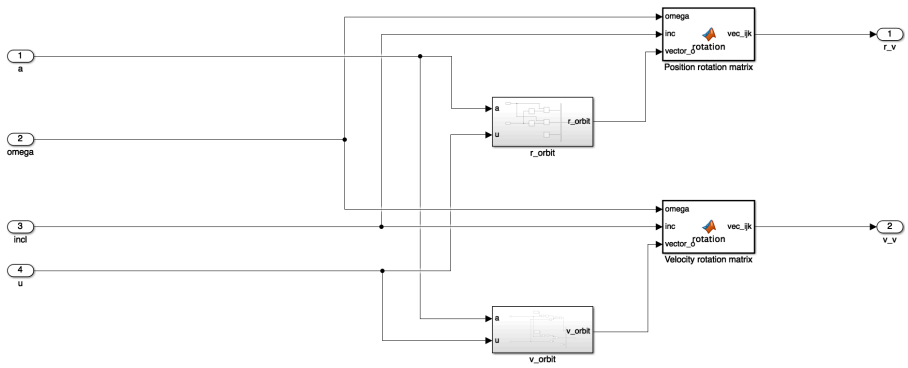


Figure 3.7: Keplerian elements to position and velocity in ECI

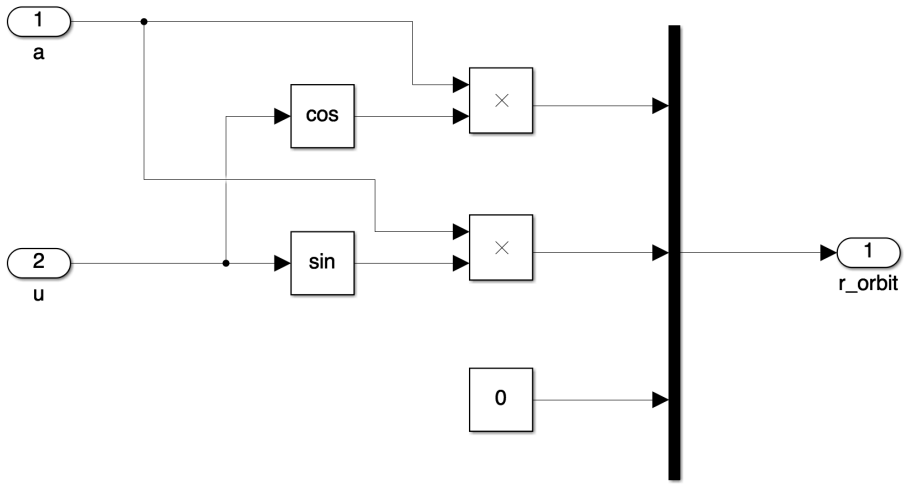


Figure 3.8: Conversion from Keplerian elements to orbital-plane position

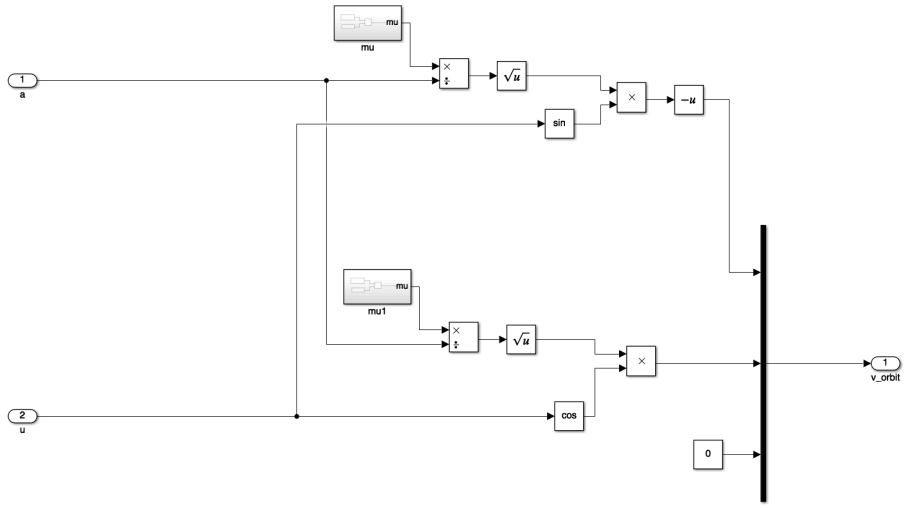


Figure 3.9: Conversion from Keplerian elements to orbital-plane velocity

3.1.1.3 Satellite frame — RSW

The last coordinate frame to be introduced is the satellite coordinate frame,[7] or RSW. This frame is used to study the relative motion between two satellites; which for this project they are the leader and the follower.

The R axis points in the same direction as the position vector, normal to the orbit. The S axis points along-track, perpendicular to R axis so the plane defined by the R and S axes is contained in the orbit.

In the present project, it is considered that the origin of the RSW coordinate frame is in the leader satellite. The follower satellite refers to the leader by means of the RSW frame as can be seen in Figure 3.10.

It is possible to transform from the ECI to RSW; however, as the later is not an inertial frame, it is necessary to account for non-inertial acceleration contributions.

[7]Vallado, *Fundamentals of Astrodynamics and Applications, 4th ed. (Space Technology Library)*.

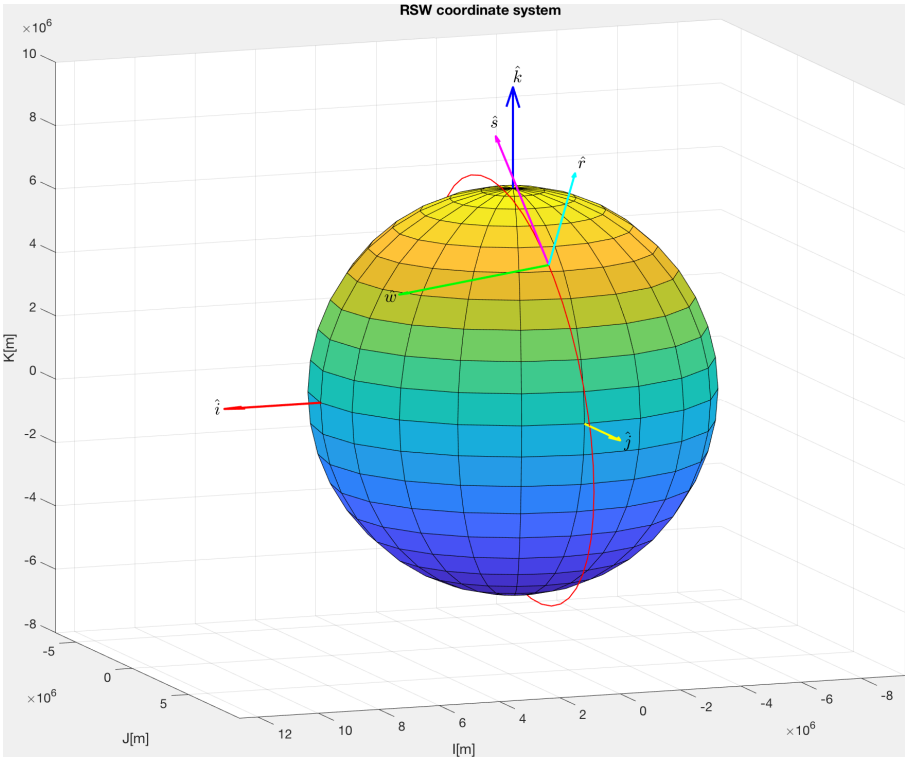


Figure 3.10: RSW coordinate system in ECI frame

The approach followed is to pre-multiply by a rotation matrix to transform between ECI and an orbit-plane reference frame $\hat{i}'\,\hat{j}'\,\hat{k}'$, and then followed by a transformation between this reference frame and RSW.[8] This helper reference frame, $\hat{i}'\,\hat{j}'\,\hat{k}'$, will be identified by IJK' (in Matlab™ as IJKP), and it serves just as an intermediate step between ECI and RSW.

This orbital plane IJK' is subject to precession and therefore it would be necessary to account for its rotation as the Earth orbits around the sun. As the proposed orbit is sun-synchronous, the precession is fixed to the time to perform one rotation in one year, i.e. $\dot{\Omega} = \frac{2\pi}{199.23 \times 10^{-9}\,\mathrm{s}}$. As the precession is very slow it has been considered also quasi-inertial. Figure 3.11 shows the effects of precession in the orbit.

Other effects on the coordinate transformations, e.g. nutation, are considered small enough in the scope of this project; however, specific assessments shall be performed for each project.

The following elemental rotation matrices follow the sign criteria of Vallado,[9]

[8] Vallado, *Fundamentals of Astrodynamics and Applications, 4th ed. (Space Technology Library)*.
[9] Ibid.

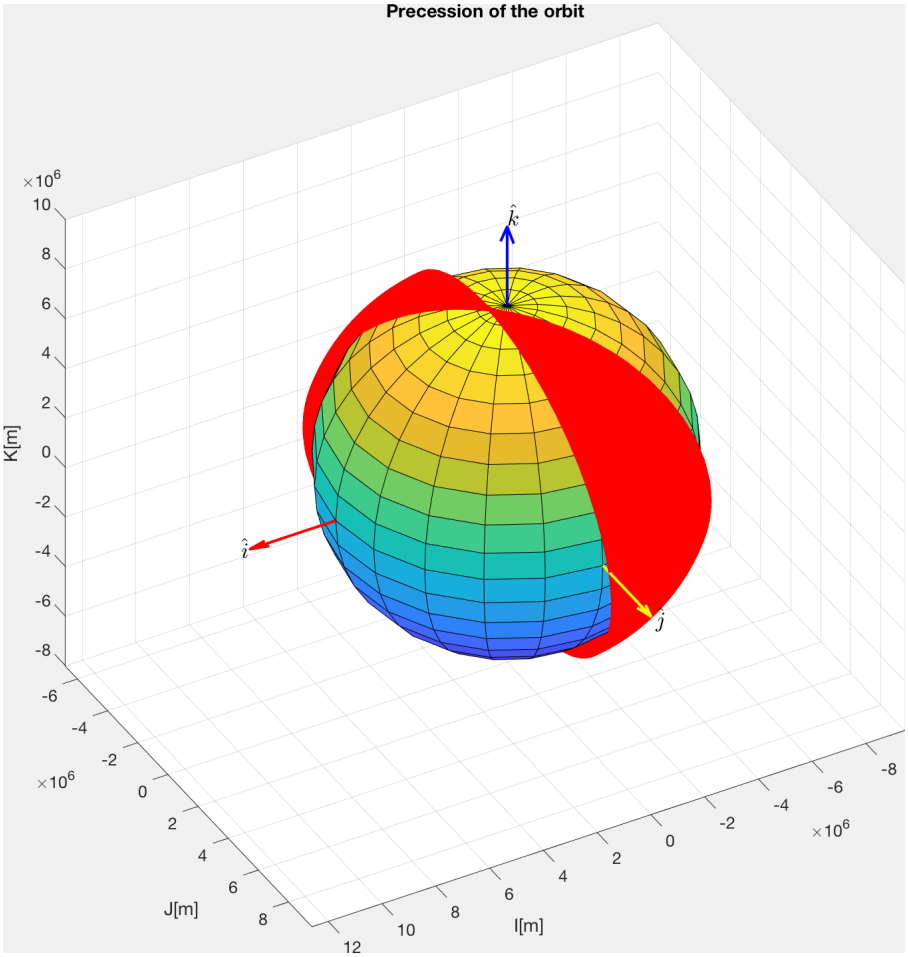


Figure 3.11: Orbit precession in ECI frame

$$\mathbf{ROT}_1(\alpha) = \begin{pmatrix} 1 & 0 & 0 \\ 0 & \cos(\alpha) & \sin(\alpha) \\ 0 & -\sin(\alpha) & \cos(\alpha) \end{pmatrix} \tag{3.12a}$$

$$\mathbf{ROT}_2(\alpha) = \begin{pmatrix} \cos(\alpha) & 0 & -\sin(\alpha) \\ 0 & 1 & 0 \\ \sin(\alpha) & 0 & \cos(\alpha) \end{pmatrix} \tag{3.12b}$$

$$\mathbf{ROT}_3(\alpha) = \begin{pmatrix} \cos(\alpha) & \sin(\alpha) & 0 \\ -\sin(\alpha) & \cos(\alpha) & 0 \\ 0 & 0 & 1 \end{pmatrix} \tag{3.12c}$$

(3.12d)

From IJK' to ECI, for the sun-synchronous orbit proposed, the vectors can be obtained by the matrix,[10]

[10]Vallado, *Fundamentals of Astrodynamics and Applications, 4th ed. (Space Technology Library)*.

$$\mathbf{M}_{ijk'}^{eci} = \mathbf{ROT}_3\left(-\frac{\pi}{2} - \dot{\Omega}t\right) \cdot \mathbf{ROT}_1(-i) \tag{3.13}$$

Note that the argument $\left(-\frac{\pi}{2} - \dot{\Omega}t\right)$, of matrix $\mathbf{ROT}_3$, takes into account the precession of the orbit. With this matrix, and its transpose, it is possible to perform the following transformations,

$$\vec{\mathbf{r}}_{ijk'} = \mathbf{M}_{eci}^{ijk'} \cdot \vec{\mathbf{r}}_{eci} \tag{3.14}$$

$$\vec{\mathbf{r}}_{eci} = \mathbf{M}_{ijk'}^{eci} \cdot \vec{\mathbf{r}}_{ijk'} \tag{3.15}$$

As both frames are considered quasi-inertial, the transformation for the velocity and acceleration follows the same criteria,

$$\vec{\mathbf{r}}_{ijk'} = \mathbf{M}_{eci}^{ijk'} \cdot \vec{\mathbf{r}}_{eci} \tag{3.16}$$

$$\vec{\mathbf{v}}_{ijk'} = \mathbf{M}_{eci}^{ijk'} \cdot \vec{\mathbf{v}}_{eci} \tag{3.17}$$

$$\vec{\mathbf{a}}_{ijk'} = \mathbf{M}_{eci}^{ijk'} \cdot \vec{\mathbf{a}}_{eci} \tag{3.18}$$

From IJK' to RSW, the transformation needs to take into account the rotation of the coordinate system,[11]

$$\mathbf{M}_{ijk'}^{rsw} = \mathbf{ROT}_3(u) = \mathbf{ROT}_3(\omega_{sat} \cdot t) \tag{3.19}$$

where ω_{sat} is the angular velocity of the satellite around Earth and for circular orbits is constant,

$$\omega_{sat} = \sqrt{\frac{\mu}{\|\vec{\mathbf{r}}_{eci}\|^3}} \tag{3.20}$$

and μ is the gravitational parameter $G \cdot m_{\oplus}$.

Therefore, with the above definitions, and their transposes, it is possible to construct a set of equations that transform from IJK' to RSW.

$$\vec{\mathbf{r}}_{rsw} = \mathbf{M}_{ijk'}^{rsw}\left(\vec{\mathbf{r}}_{ijk'} - \vec{\mathbf{r}}_o\right) \tag{3.21}$$

$$\vec{\mathbf{v}}_{rsw} = \mathbf{M}_{ijk'}^{rsw}\left(\vec{\mathbf{v}}_{ijk'} - \vec{\mathbf{v}}_o\right) - \mathbf{M}_{ijk'}^{rsw}\frac{\mathrm{d}}{\mathrm{d}t}\left(\mathbf{M}_{rsw}^{ijk'}\right)\vec{\mathbf{r}}_{rsw} \tag{3.22}$$

$$\vec{\mathbf{a}}_{rsw} = \mathbf{M}_{ijk'}^{rsw}\left(\vec{\mathbf{a}}_{ijk'} - \vec{\mathbf{a}}_o\right) - \mathbf{M}_{ijk'}^{rsw}2\frac{\mathrm{d}}{\mathrm{d}t}\left(\mathbf{M}_{rsw}^{ijk'}\right)\vec{\mathbf{v}}_{rsw} - \mathbf{M}_{ijk'}^{rsw}\frac{\mathrm{d}^2}{\mathrm{d}t^2}\left(\mathbf{M}_{rsw}^{ijk'}\right)\vec{\mathbf{r}}_{rsw} \tag{3.23}$$

where $\vec{\mathbf{r}}_o$, $\vec{\mathbf{v}}_o$ and $\vec{\mathbf{a}}_o$ are the position, velocity and acceleration of the RSW frame origin, which is the leader satellite.

[11] Vallado, *Fundamentals of Astrodynamics and Applications, 4th ed. (Space Technology Library)*.

The opposite transformation, from RSW to ECI, is only necessary for the external thruster contribution, which will be added by the DKE to the rest of the contributions; therefore, the thruster acceleration vector is transformed by the following equation,

$$\vec{\mathbf{a}}_{t_{eci}} = \mathbf{M}_{ijk'}^{eci} \cdot \mathbf{M}_{rsw}^{ijk'} \cdot \vec{\mathbf{a}}_{t_{rsw}} \tag{3.24}$$

It is important to note that although the precession has been taken into account, the coordinate system transformations have been simplified. Depending on the scope of the work at hand it might be necessary to take into account other effects that in the long run might not be negligible.

3.1.2 Dynamics, Kinetics and Environment

The dynamics of satellite motion are modeled by integrating a selected group of accelerations in the ECI frame, they are:

- The two-body acceleration from Newtonian mechanics, between Earth and the satellite.
- The J2 gravity field perturbation due to the oblateness of the Earth. This perturbation is responsible for the precession of the orbit in ECI frame, the one that keeps the orbit sun-synchronous.
- The atmospheric drag.

The two-body acceleration equation, from Newtonian mechanics is,[12]

$$\frac{\mathrm{d}^2\vec{\mathbf{r}}}{\mathrm{d}t^2} = \ddot{\vec{\mathbf{r}}} = -\frac{\mu}{\|\vec{\mathbf{r}}\|^2}\frac{\vec{\mathbf{r}}}{\|\vec{\mathbf{r}}\|} \tag{3.25}$$

The J2 zonal harmonic adds a gravity field perturbation to take into account the oblateness of the Earth.[13] Its model and the required coordinate system transformations, are both provided by Matlab™ and Simulink™.[14] The Simulink™ block includes the two-body acceleration; however, in order to assess both contributions separately, the two-body acceleration has been subtracted from the J2 zonal harmonic block.

The atmospheric drag equation is defined as follows,[15]

$$\vec{\mathbf{a}}_{drag} = -\frac{1}{2}\frac{c_D A \rho v_{rel}^2}{m_{sat}}\frac{\vec{\mathbf{v}}_{rel}}{\|\vec{\mathbf{v}}_{rel}\|} \tag{3.26}$$

where,

[12] Vallado, *Fundamentals of Astrodynamics and Applications, 4th ed. (Space Technology Library)*.
[13] Ibid.
[14] Inc The MathWorks, *Aerospace Blockset User's Guide R2018a* (Natick, Massachusetts, 2018).
[15] Vallado, *Fundamentals of Astrodynamics and Applications, 4th ed. (Space Technology Library)*.

c_D It is the coefficient of drag and depends on the geometry of the satellite. An initial approximation[16] of a constant 2.2 has been used.

A It is the cross sectional area perpendicular to the motion. In the nominal case, the satellite has the side with area $height \times width$ facing the motion.

ρ It is the atmospheric density. It depends on many factors and it is a model difficult to implement accurately. Therefore, the model[17] provided by Simulink™ is used, which is based on the 2001 United States Naval Research Laboratory Mass Spectrometer and Incoherent Scatter Radar Exosphere. It takes into account total air density and anomalous oxygen.

m_{sat} Mass of the satellite in order to obtain an acceleration.

$\vec{\mathbf{v}}_{rel}$ The velocity of the satellite relative to the atmosphere. It is necessary to take into account that the atmosphere has a rotation profile due to Earth's own rotation. This relative velocity is defined as[18] $\vec{\mathbf{v}}_{rel} = \dot{\vec{\mathbf{r}}} - \left(\omega_{\oplus} \times \vec{\mathbf{r}}\right)$.

Other acceleration contributions are considered to be small enough in the present scenario that are not included in the DKE model. These are: Higher order zonal harmonics, third body and solar radiation pressure.

Having all the contributing accelerations, Cowell's formulation[19] is used to integrate twice, obtaining velocity and position,

$$\ddot{\vec{\mathbf{r}}} = -\frac{\mu}{\|\vec{\mathbf{r}}\|^2}\frac{\vec{\mathbf{r}}}{\|\vec{\mathbf{r}}\|} + \sum \vec{\mathbf{a}} \tag{3.27}$$

The DKE modeled after Cowell's formulation is depicted in Figure 3.12. Each acceleration contribution has been modeled independently:

- Two body model in Figure 3.13
- J2 Zonal Harmonic in Figure 3.14
- Drag model in Figure 3.15, with the atmospheric density model in Figure 3.16.

The leader DKE model is slightly different than the follower. It is considered that the leader has thrusters that compensate for atmospheric drag, therefore, this block has been removed. The rest remains the same.

This model of the DKE is used to perform a simulation which is considered more representative than the linearized model of the plant of section §3.1.3.

[16] Vallado, *Fundamentals of Astrodynamics and Applications, 4th ed. (Space Technology Library)*.
[17] The MathWorks, *Aerospace Blockset User's Guide R2018a*.
[18] Vallado, *Fundamentals of Astrodynamics and Applications, 4th ed. (Space Technology Library)*.
[19] Ibid.

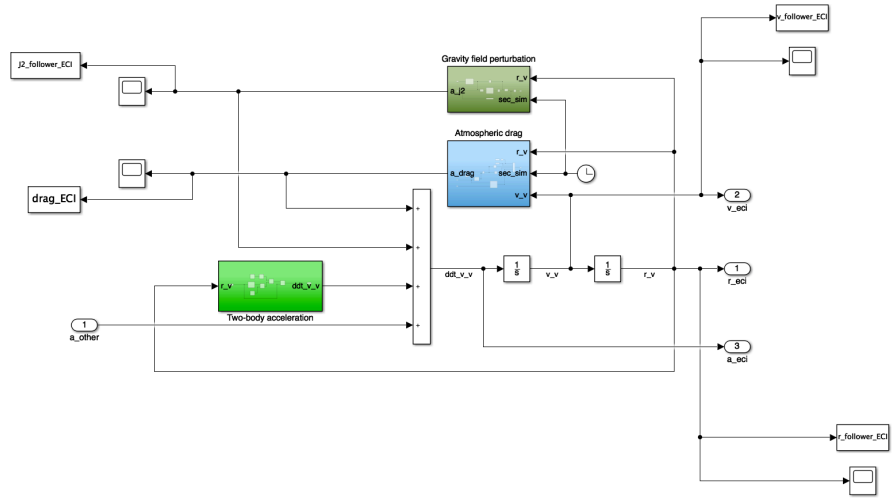


Figure 3.12: Overview of the DKE Simulink™ model

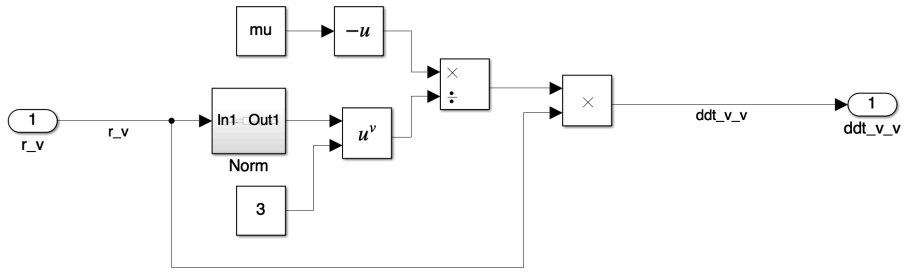


Figure 3.13: Model of the two-body acceleration

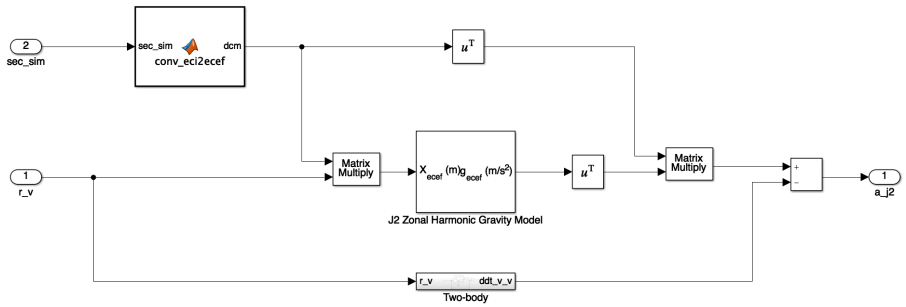


Figure 3.14: J2 zonal harmonic model

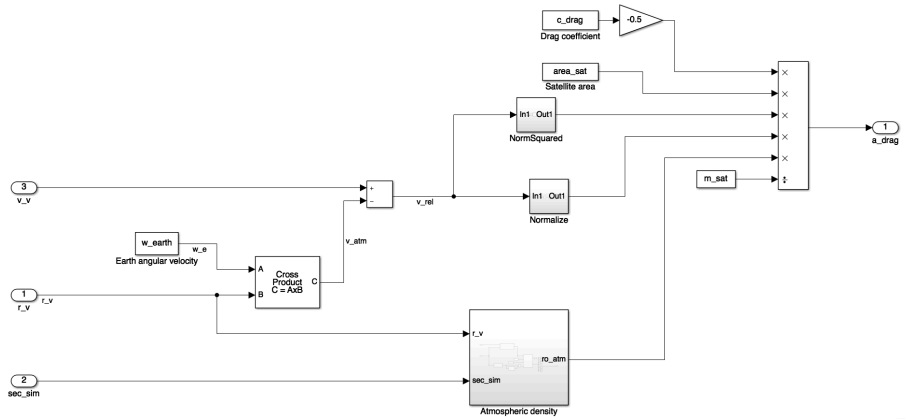


Figure 3.15: Atmospheric drag model

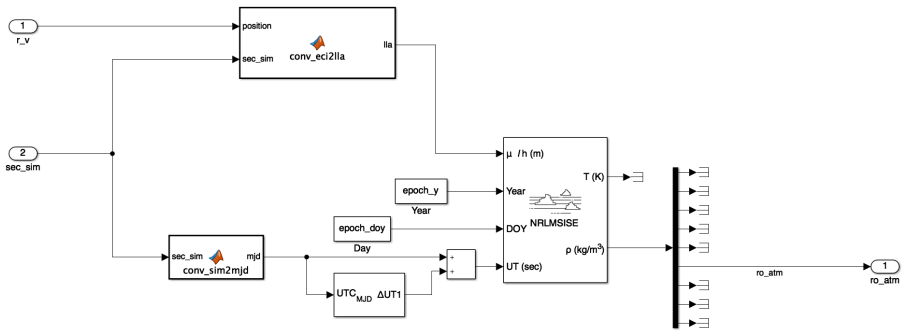


Figure 3.16: Atmospheric density model

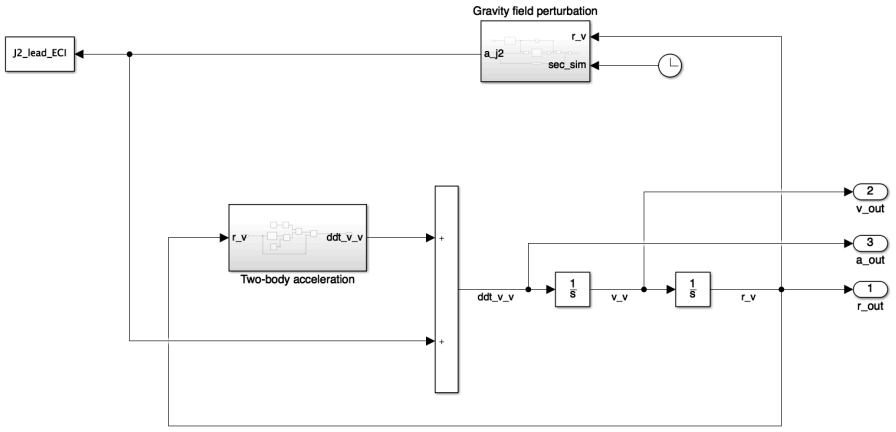


Figure 3.17: Leader satellite model

3.1.3 Hill-Clohessy-Wiltshire equations

The model of the DKE from section §3.1.2 cannot be used directly as the plant with the intention of obtaining the control system. Following the research of George Hill's in Lunar Theory,[20] W. H. Clohessy and R. S. Wiltshire[21] created a set of linearized equations of relative motion that can be used to describe formation flying in the RSW frame.[22] These equations —hereafter HCW equations— are only valid for near circular orbits.[23]

For HCW equations in the RSW frame, with the leader satellite acting as the origin of coordinates, the x component represent the magnitude in the R axis, the y component in the S axis and the z component in the W axis. The dot operator represents the derivative with respect to time,

[20] George W. Hill, "Researches in Lunar Theory," *American Journal of Mathematics* 1: 5-26 (1878).

[21] W. H. Clohessy and R. S. Wiltshire, "Terminal Guidance System for Satellite Rendezvous," *Journal of the Aerospace Sciences* 27: 653-674 (1960).

[22] Angulo Jerez et al., "Control de Formaciones en Vuelo de Satélites de Bajo Coste."

[23] Vallado, *Fundamentals of Astrodynamics and Applications, 4th ed. (Space Technology Library)*.

$$\ddot{x} - 2\omega\dot{y} - 3\omega^2 x = a_x \tag{3.28a}$$

$$\ddot{y} + 2\omega\dot{x} = a_y \tag{3.28b}$$

$$\ddot{z} + \omega^2 z = a_z \tag{3.28c}$$

where a_x, a_y and a_z are the accelerations due to external applied forces, and $\omega = \sqrt{\frac{\mu}{r^3}}$ is the leader satellite's orbital angular velocity, which is a constant in circular orbits. Note that equations (3.28a) and (3.28b) are coupled.

In the proposed orbital configuration of leader/follower, the follower has a negative y component.

3.2 Control system modeling

In order to obtain a model of the HCW equations suitable for Simulink™ it is necessary to obtain the transfer function.[24] If the Laplace transforms of the relevant variables are defined as,

$$\mathscr{L}\big(x(t)\big) = X(s) \tag{3.29a}$$

$$\mathscr{L}\big(y(t)\big) = Y(s) \tag{3.29b}$$

$$\mathscr{L}\big(z(t)\big) = Z(s) \tag{3.29c}$$

$$\mathscr{L}\big(a_x(t)\big) = A_x(s) \tag{3.29d}$$

$$\mathscr{L}\big(a_y(t)\big) = A_y(s) \tag{3.29e}$$

$$\mathscr{L}\big(a_z(t)\big) = A_z(s) \tag{3.29f}$$

The Laplace transform of equations (3.28) results in,

$$s^2 X(s) - s x_o - \dot{x}_o - 2\omega s Y(s) + y_o - 3\omega^2 X(s) = A_x(s) \tag{3.30a}$$

$$s^2 Y(s) - s y_o - \dot{y}_o + 2\omega s X(s) - x_o = A_y(s) \tag{3.30b}$$

$$s^2 Z(s) - s\, z_o - \dot{z}_o + \omega^2 Z(s) = A_z(s) \tag{3.30c}$$

Assuming initial positions and velocities equal to zero in equations (3.30) results in,

$$s^2 X(s) - 2\omega s Y(s) - 3\omega^2 X(s) = A_x(s) \tag{3.31a}$$

$$s^2 Y(s) + 2\omega s X(s) = A_y(s) \tag{3.31b}$$

$$s^2 Z(s) + \omega^2 Z(s) = A_z(s) \tag{3.31c}$$

[24] Franklin, Powell, and Emami-Naeini, *Feedback Control of Dynamic Systems, 4th Edition*.

that, for the steady state, can be solved in the form,

$$\begin{pmatrix} X(s) \\ Y(s) \\ Z(s) \end{pmatrix} = \mathbf{T(s)} \begin{pmatrix} A_x(s) \\ A_y(s) \\ A_z(s) \end{pmatrix} \tag{3.32}$$

where $\mathbf{T(s)}$ is,

$$\mathbf{T(s)} = \begin{pmatrix} \frac{1}{s^2+\omega^2} & \frac{2\omega}{s(s^2+\omega^2)} & 0 \\ -\frac{2\omega}{s(s^2+\omega^2)} & \frac{s^2-3\omega^2}{s^2(s^2+\omega^2)} & 0 \\ 0 & 0 & \frac{1}{s^2+\omega^2} \end{pmatrix} \tag{3.33}$$

The transfer function (3.33) can be represented in state-space form,[25]

$$\dot{\vec{\mathbf{p}}} = \mathbf{F}\vec{\mathbf{p}} + \mathbf{G}\vec{\mathbf{u}} \tag{3.34a}$$

$$\vec{\mathbf{q}} = \mathbf{H}\vec{\mathbf{p}} + \mathbf{J}\vec{\mathbf{u}} \tag{3.34b}$$

where the state-vector (3.35) contains the position and velocities of the HCW equations (3.31),

$$\vec{\mathbf{p}} = \begin{pmatrix} x & y & z & \dot{x} & \dot{y} & \dot{z} \end{pmatrix}^T \tag{3.35}$$

and the input-vector (3.36) contains the input to the system, in this case, the accelerations vector due to external forces,

$$\vec{\mathbf{u}} = \begin{pmatrix} u_x & u_y & u_z \end{pmatrix}^T \tag{3.36}$$

The matrices in (3.34) correspond to,

- $\mathbf{F}$: The system matrix.
- $\mathbf{G}$: The input matrix.
- $\mathbf{H}$: The output matrix.
- $\mathbf{J}$: The direct transmission matrix.

By means of equation[26] (3.37) and matrices (3.38), it can be verified that (3.33) and (3.34) are equivalent,

$$\mathbf{H}(s\mathbf{I} - \mathbf{F})^{-1}\mathbf{G} + \mathbf{J} = \mathbf{T(s)} \tag{3.37}$$

[25] Franklin, Powell, and Emami-Naeini, *Feedback Control of Dynamic Systems, 4th Edition*.
[26] Ibid.

$$\mathbf{F} = \begin{pmatrix} 0 & 0 & 0 & 1 & 0 & 0 \\ 0 & 0 & 0 & 0 & 1 & 0 \\ 0 & 0 & 0 & 0 & 0 & 1 \\ 3\omega^2 & 0 & 0 & 0 & 2\omega & 0 \\ 0 & 0 & 0 & -2\omega & 0 & 0 \\ 0 & 0 & -\omega^2 & 0 & 0 & 0 \end{pmatrix} \tag{3.38a}$$

$$\mathbf{G} = \begin{pmatrix} 0 & 0 & 0 \\ 0 & 0 & 0 \\ 0 & 0 & 0 \\ 1 & 0 & 0 \\ 0 & 1 & 0 \\ 0 & 0 & 1 \end{pmatrix} \tag{3.38b}$$

$$\mathbf{H} = \begin{pmatrix} 0 & 0 & 0 & 1 & 0 & 0 \\ 0 & 0 & 0 & 0 & 1 & 0 \\ 0 & 0 & 0 & 0 & 0 & 1 \end{pmatrix} \tag{3.38c}$$

$$\mathbf{J} = \begin{pmatrix} 0 & 0 & 0 \\ 0 & 0 & 0 \\ 0 & 0 & 0 \end{pmatrix} \tag{3.38d}$$

The Simulink™ model of equations (3.34) is depicted in Figure 3.18, where `HCW_ss.A`, `HCW_ss.B`, `HCW_ss.C` and `HCW_ss.D` correspond to matrices **F**, **G**, **H** and **J**, respectively.

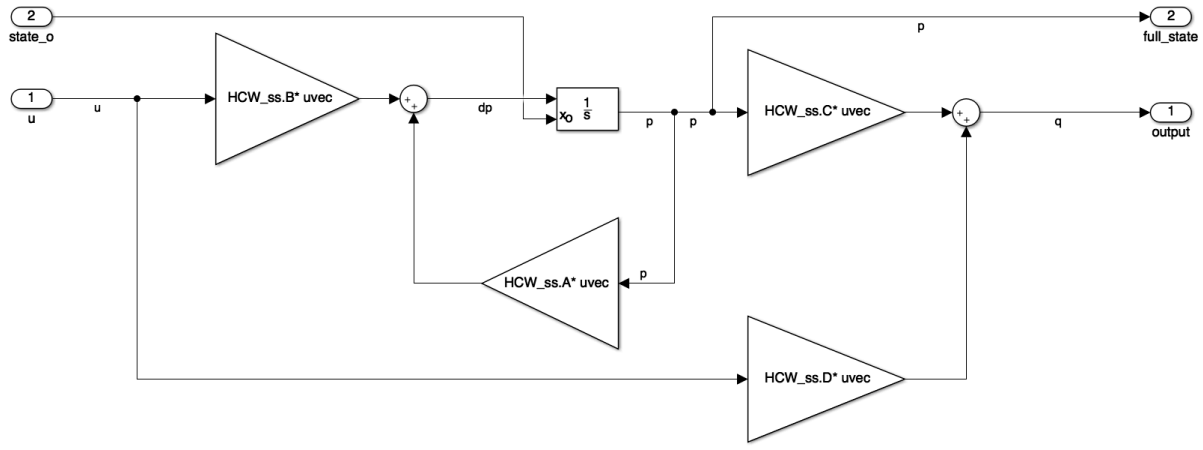


Figure 3.18: State-Space model of the plant

Having the state-space and transfer functions of the HCW equations it would be necessary to verify that a control system can indeed be created. When a system is controllable, its controllability matrix $\mathscr{C}$ is non-singular.[27] This is achieved by checking that the rank of equation (3.39) is equal to the number of states,

[27] Franklin, Powell, and Emami-Naeini, *Feedback Control of Dynamic Systems, 4th Edition*.

$$\operatorname{rank}(\mathscr{C}) = \operatorname{rank}\begin{pmatrix}\mathbf{G} & \mathbf{FG} & \cdots & \mathbf{F}^{n-1}\mathbf{G}\end{pmatrix} = 6 \tag{3.39}$$

where n is the size of $\mathbf{F}$. Therefore, the system is controllable.

An initial assessment of the behavior of the system can be performed by analyzing the poles, which are obtained by calculating the eigenvalues of $\mathbf{F}$,[28] i.e.

$$\operatorname{eig}(\mathbf{F}) = \begin{pmatrix} 0 + 0\mathrm{i} \\ 0 + 0\mathrm{i} \\ 0 + 0.0011\mathrm{i} \\ 0 - 0.0011\mathrm{i} \\ 0 + 0.0011\mathrm{i} \\ 0 - 0.0011\mathrm{i} \end{pmatrix} \tag{3.40}$$

The system presents an oscillatory behavior due to the presence of an imaginary component and the absence of real positive or negative components.[29]

With the information available, an strategy to create a controller can be devised; in this case, it is based on the error-space approach from Franklin, Powell, and Emami-Naeini.[30] In this approach, the control has to follow a reference input profile with no steady-state error, and reject disturbances. The case presented below considers only a static, constant reference, which simplifies the equations. Nevertheless, this approach can be extended if necessary by including a profile for the reference and disturbances.

Suppose the plant represented by the following system of equations,[31]

$$\dot{\vec{\mathbf{p}}} = \mathbf{F}\vec{\mathbf{p}} + \mathbf{G}\vec{\mathbf{u}} \tag{3.41a}$$

$$\vec{\mathbf{q}} = \mathbf{H}\vec{\mathbf{p}} \tag{3.41b}$$

The tracking error is defined as,[32]

$$\vec{\mathbf{e}} = \vec{\mathbf{q}} - \vec{\mathbf{r}} \tag{3.42}$$

With a static reference input,

$$\dot{\vec{\mathbf{r}}} = 0 \tag{3.43}$$

The intention is to regulate this error so it tends to zero with sufficient amount of time, even in the presence of small perturbations.[33]

[28] Franklin, Powell, and Emami-Naeini, *Feedback Control of Dynamic Systems, 4th Edition*.
[29] Ibid.
[30] Ibid.
[31] Ibid.
[32] Ibid.
[33] Ibid.

Substituting (3.42) into (3.43), and identifying with (3.41b), the error can be calculated in terms of the state,[34]

$$\dot{\vec{\mathbf{e}}} = \dot{\vec{\mathbf{q}}} \tag{3.44}$$

$$\dot{\vec{\mathbf{e}}} = \mathbf{H}\dot{\vec{\mathbf{p}}} \tag{3.45}$$

Now, the state vector can be substituted by the error state defined by,[35]

$$\vec{\xi} = \dot{\vec{\mathbf{p}}} \tag{3.46}$$

$$\dot{\vec{\xi}} = \ddot{\vec{\mathbf{p}}} \tag{3.47}$$

and the input, by the input in the error space defined by,[36]

$$\vec{\mu} = \dot{\vec{\mathbf{u}}} \tag{3.48}$$

With the definitions given above, equation (3.45) is has the form,[37]

$$\dot{\vec{\mathbf{e}}} = \mathbf{H}\vec{\xi} \tag{3.49}$$

and the state equation would be then,[38]

$$\dot{\vec{\xi}} = \mathbf{F}\vec{\xi} + \mathbf{G}\vec{\mu} \tag{3.50}$$

Equations (3.50) and (3.49) describe the system in an error-space, following a static, constant reference. These equations can be rewritten in a standard state-variable form,

$$\dot{\vec{\mathbf{z}}} = \mathbf{A}\vec{\mathbf{z}} + \mathbf{B}\vec{\mu} \tag{3.51}$$

where,

$$\vec{\mathbf{z}} = \begin{pmatrix} \vec{\mathbf{e}} & \vec{\xi} \end{pmatrix}^T \tag{3.52}$$

$$\mathbf{A} = \begin{pmatrix} \vec{\mathbf{0}} & \mathbf{H} \\ \vec{\mathbf{0}} & \mathbf{F} \end{pmatrix} \tag{3.53}$$

$$\mathbf{B} = \begin{pmatrix} \vec{\mathbf{0}} \\ \mathbf{G} \end{pmatrix} \tag{3.54}$$

[34]Franklin, Powell, and Emami-Naeini, *Feedback Control of Dynamic Systems, 4th Edition*.
[35]Ibid.
[36]Ibid.
[37]Ibid.
[38]Ibid.

According to the method, if **F** and **G** are controllable, and do not have a zero in the same place as a root of the characteristic equation of the reference signal, i.e. $\alpha_r(s) = s$, then the error-space system is controllable;[39] which is the case as the plant represented by (3.41) and (3.38) do not have zeros (for example, running the Matlab™ command `tzero()`,[40] returns an empty vector).

Therefore, a control law can be obtained in the form of (3.55) that can be given an arbitrary dynamic by pole placement,[41]

$$\vec{\mu} = -\begin{pmatrix}\mathbf{K_1} & \mathbf{K_0}\end{pmatrix}\begin{pmatrix}\vec{\mathbf{e}} \\ \vec{\xi}\end{pmatrix} = -\mathbf{K}\vec{\mathbf{z}} \tag{3.55}$$

The last part of the method is to be able to use the control obtained for the error-space system in the original state-space system. Franklin, Powell, and Emami-Naeini formulation accommodates any reference and disturbance differential equations, leading to a more general solution; in this case, a constant reference input was used in (3.43), which reduces the solution to (3.56). In summary, the equation (3.56) represents the control law of (3.55) in terms of the original plant in state-space form,[42]

$$\vec{\mathbf{u}} = -\mathbf{K_1}\int^{t} e\,\mathrm{d}t - \mathbf{K_0}\vec{\mathbf{p}} \tag{3.56}$$

The Simulink™ block diagram of Figure 3.19 shows the final disposition of the control elements according to this method.[43]

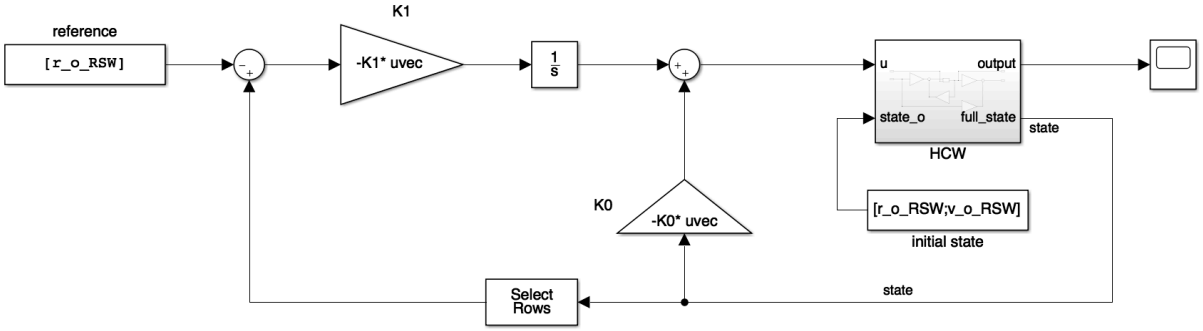


Figure 3.19: Control model using error-space

The pole selection method to obtain the desired matrices $\mathbf{K_0}$ and $\mathbf{K_1}$ is based on a second order dominant pole placement.[44] It has been performed mostly by qualitative assessment and simulation of various cases. The intention is to attain the desired characteristics of overshoot and settling time, that should be compatible with the performances of commercial electric propulsion

[39] Franklin, Powell, and Emami-Naeini, *Feedback Control of Dynamic Systems, 4th Edition*.
[40] Inc The MathWorks, *Control System Toolbox Reference R2018a* (Natick, Massachusetts, 2018).
[41] Franklin, Powell, and Emami-Naeini, *Feedback Control of Dynamic Systems, 4th Edition*.
[42] Ibid.
[43] Ibid.
[44] Ibid.

thrusters for CubeSats. Nevertheless, the performances required depend on the mission, and a specific tunning shall be performed in each case.

It is possible to calculate the desired poles with the following equations,[45]

$$\omega_n = \frac{4}{\zeta t_s} \tag{3.57}$$

$$\sigma = \zeta \omega_n \tag{3.58}$$

$$\omega_d = \pm \sqrt{1 - \zeta^2} \tag{3.59}$$

$$\text{pole} = -\sigma \pm j\omega_d \tag{3.60}$$

where ω_n is the natural frequency, σ is the real part of the pole and ω_d is the imaginary part of the pole (and also the damped frequency).

The following nominal scenario is then proposed.

- Settling time: $t_s = 2807\,\text{s} \approx \frac{\lambda_{orbit}}{2}$
- Damping ratio: $\zeta = \sin(45) \approx 5\,\%_{\text{os}}$[46]

The rationale behind these figures is to obtain a relatively stable behavior and keeping the maximum required thrust under 1 mN. It is important to note that shorter distances between leader and follower or longer settling times, effectively reduce the required thrust; please refer to §3.3, for a comparative.

For the above conditions, in order to calculate **K** with the desired closed-loop poles, the Matlab™ instruction `place()`[47,48] is used. This instruction requires as many poles as the dimension of the **A** matrix, and such poles cannot be in the same place.

Equation (3.60) gives two poles, it is then suggested to place other seven fast poles far away in the negative part of the real axis, it is considered that four times the undamped natural frequency is enough.[49]

```
1 A = [[zeros(3); zeros(6,3)] [HCW_ss.C; HCW_ss.A]];
2 B = [zeros(3,3); HCW_ss.B];
3 z = sind(45);
4 st = orbit_period/2;
5 w_n = 4/(z*st)
6 sg = z*w_n;
7 w_d = w_n*sqrt(1-z^2);
```

[45] Franklin, Powell, and Emami-Naeini, *Feedback Control of Dynamic Systems, 4th Edition*.
[46] Ibid.
[47] The MathWorks, *Control System Toolbox Reference R2018a*.
[48] Franklin, Powell, and Emami-Naeini, *Feedback Control of Dynamic Systems, 4th Edition*.
[49] Ibid.

```
% place() cannot insert multiple poles at the same place. slightly move each
    one.
far_pole = -4*w_n;
pc = [-sg+1j*w_d;-sg-1j*w_d;far_pole;far_pole-1e-6;far_pole-2e-6;far_pole-3e-6;
    far_pole-4e-6;far_pole-5e-6;far_pole-6e-6];
K = place(A,B,pc);
K1 = K(:,1:3);
K0 = K(:,4:9);
```

Therefore, for the code above, the resulting poles are,

$$\begin{pmatrix} (-1.4247 + 1.4247\mathrm{i}) \times 10^{-3} \\ (-1.4247 - 1.4247\mathrm{i}) \times 10^{-3} \\ -8.0593 \times 10^{-3} \\ -8.0603 \times 10^{-3} \\ -8.0613 \times 10^{-3} \\ -8.0623 \times 10^{-3} \\ -8.0633 \times 10^{-3} \\ -8.0643 \times 10^{-3} \\ -8.0653 \times 10^{-3} \end{pmatrix} \tag{3.61}$$

and the matrices K_0 and K_1 calculated by `place()` are,

$$\mathbf{K_0} = \begin{pmatrix} 198.7953 \times 10^{-6} & -4.8854 \times 10^{-18} & 7.9413 \times 10^{-18} & 24.1892 \times 10^{-3} & 2.2379 \times 10^{-3} & 492.5090 \times 10^{-18} \\ 0 & 111.0157 \times 10^{-6} & -32.4502 \times 10^{-6} & -2.2379 \times 10^{-3} & 18.9774 \times 10^{-3} & -2.0124 \times 10^{-3} \\ 0 & 32.6655 \times 10^{-6} & 63.6443 \times 10^{-6} & 0 & 2.0264 \times 10^{-3} & 16.1180 \times 10^{-3} \end{pmatrix} \tag{3.62}$$

$$\mathbf{K_1} = \begin{pmatrix} 524.2047 \times 10^{-9} & -19.6892 \times 10^{-21} & 32.0119 \times 10^{-21} \\ 0 & 185.5545 \times 10^{-9} & -130.8189 \times 10^{-9} \\ 0 & 131.6429 \times 10^{-9} & -412.5496 \times 10^{-12} \end{pmatrix} \tag{3.63}$$

The present project focuses on the steady state behavior and small corrections of the reference point. Therefore, the initial state of the integrator has been manually set in order to obtain a steady state in the beginning of the simulation, from which further analysis can be performed.

3.3 Integrated system

In order to tune tune different t_s and ζ parameters, to comply with the desired actuator performances, the system in Figure 3.20 has been created.

In this model, the simulation time can start before zero in order to achieve steady-state, and then at t=0, change the reference set point in −2 %. In this way the resulting position, velocity and thrust diagrams can represent the effects of a small correction starting from a true steady-state. This capability, however, is not available in the DKE due to how it is constructed.

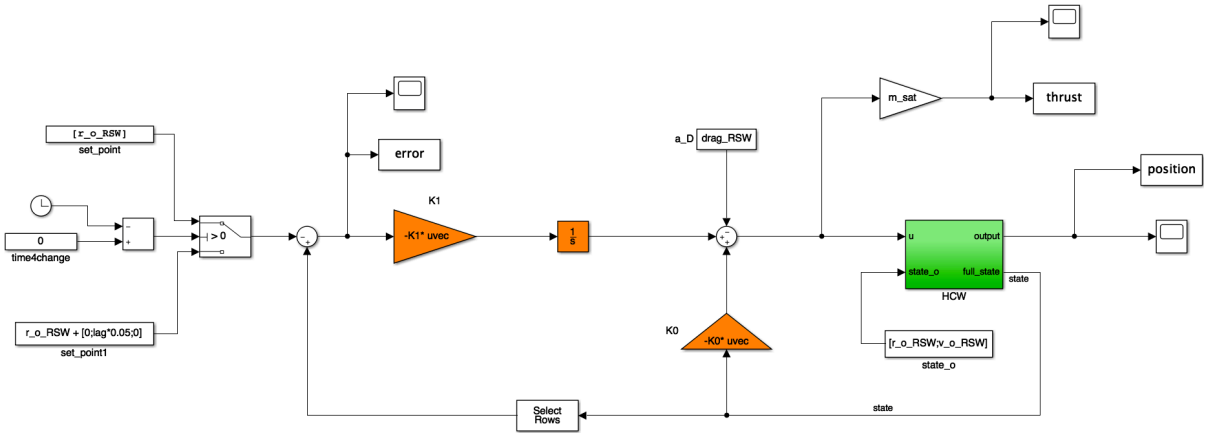


Figure 3.20: Simulink™ model for parameter tuning

Please note that at the beginning of the simulation, there is a startup transient, not shown in the figures below in order to keep them clear. The transient magnitude and settling time depend on the initial conditions of the different model elements, e.g. initial integrator values. These initial conditions have been adjusted as much as possible, however, the startup transient is still important. Therefore, the simulation time has been extended long enough to reach a steady state before performing any action on the reference set point.

Two cases have been analyzed:

1. Case 1 — Proposed nominal case:
   - $r(t < 0) = -200\,\text{m}\ \hat{s}_{rsw}$,
   - $r(t \geq 0) = -196\,\text{m}\ \hat{s}_{rsw}$,
   - $t_s = 2807\,\text{s} \approx \frac{\lambda_{orbit}}{2}$ and
   - $\zeta = \sin(45) \approx 5\,\%_{\text{os}}$.
2. Case 2 — Alternative case:
   - $r(t < 0) = -200\,\text{m}\ \hat{s}_{rsw}$,
   - $r(t \geq 0) = -196\,\text{m}\ \hat{s}_{rsw}$,
   - $t_s = 1403\,\text{s} \approx \frac{\lambda_{orbit}}{4}$ and
   - $\zeta = \sin(45) \approx 5\,\%_{\text{os}}$.

Where r is the reference set point and $\lambda_{orbit} = 5615\,\text{s}$ is the orbit period.

3.3.1 Case 1: Proposed nominal case

Figure 3.21, shows the initial S axis position of the follower satellite in $t = 0$, and its response to a change in set point. Figure 3.22 shows the remaining two axes. Figure 3.23 shows the error response to this change. It can be seen that it closely follows the profile required in Case 1 (above).

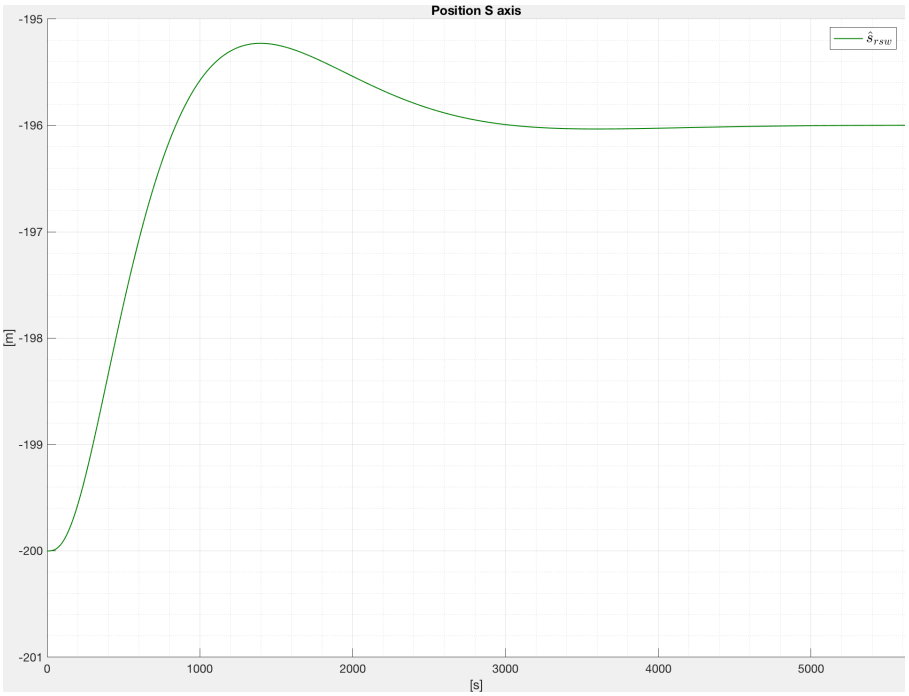


Figure 3.21: Case 1 — Position response in S axis

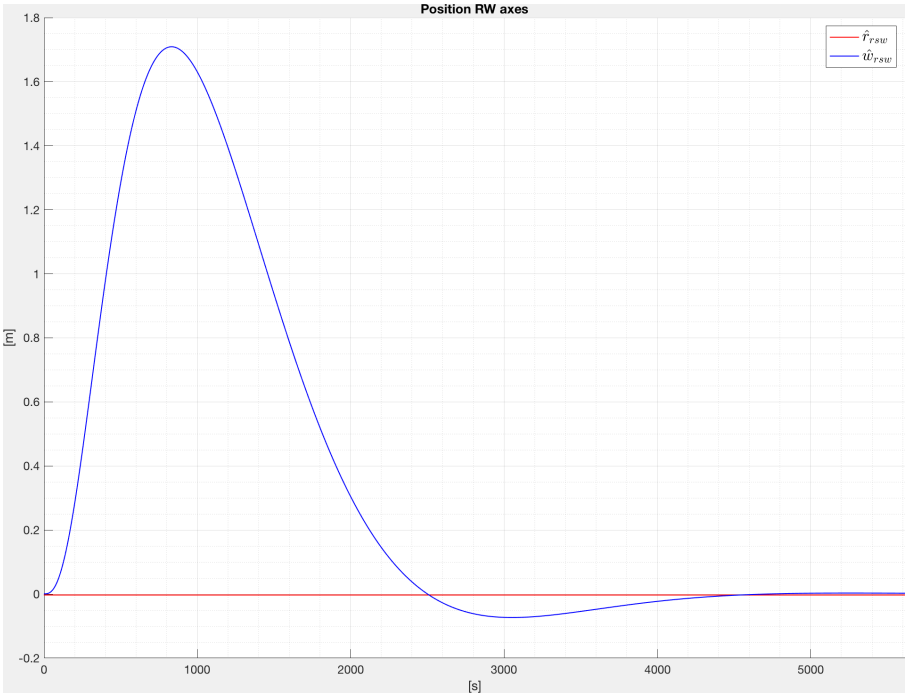


Figure 3.22: Case 1 — Position response in RW axes

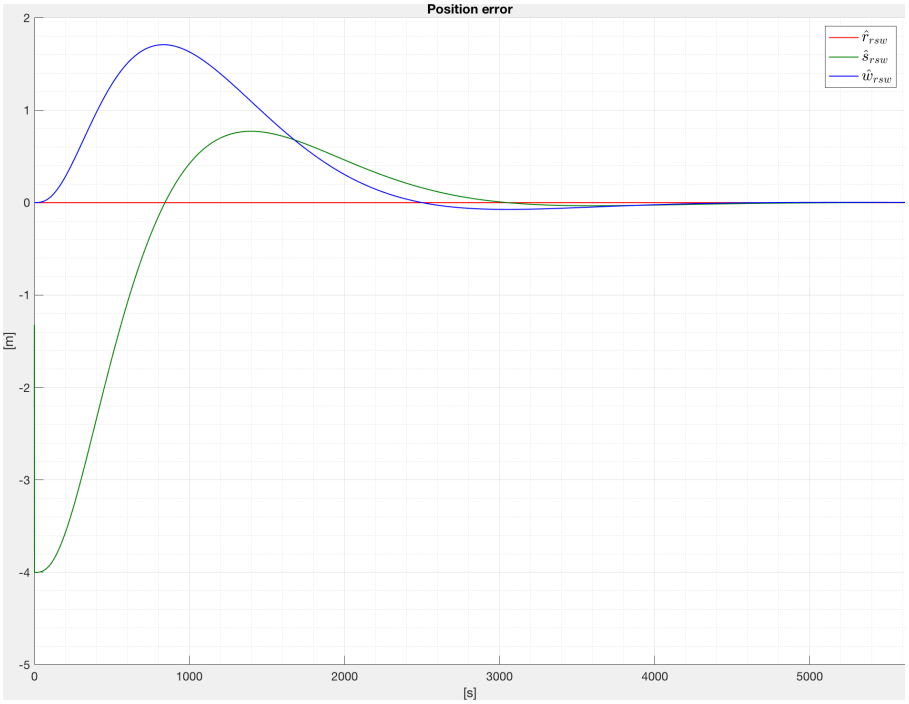


Figure 3.23: Case 1 — Error response

In Figure 3.24, the thrust required to perform this maneuver can be observed. It has a peak around 360×10^{-6} µN in the S axis. The steady state thrust demand is negligible in this model because the effects of J2 and drag are not modeled in the plant. They will be apparent in the simulations of §4.

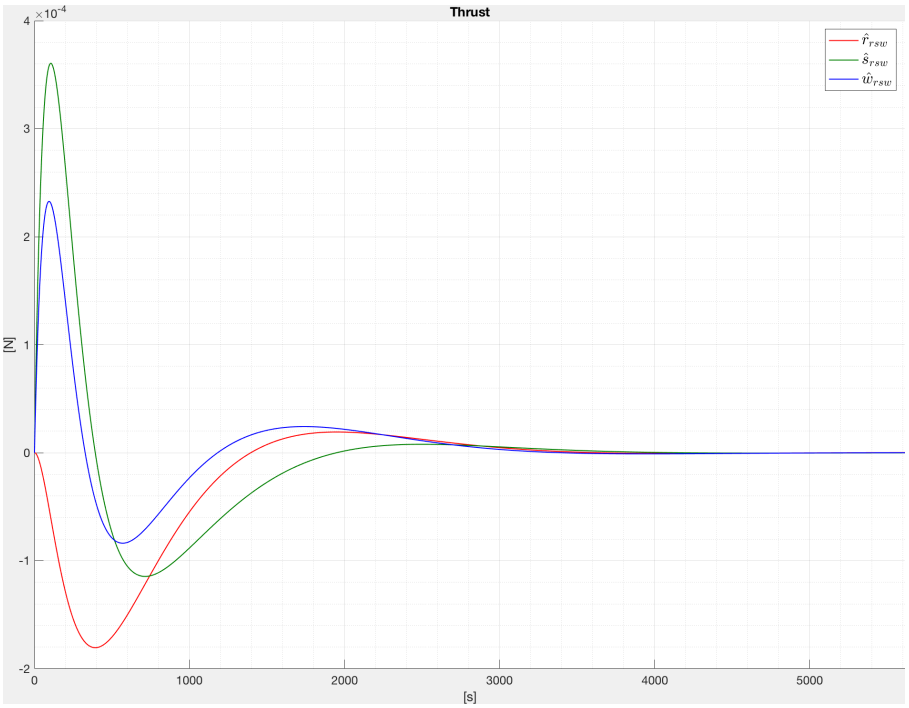


Figure 3.24: Case 1 — Thrust response

3.3.2 Case 2: Alternative case

In the alternative scenario of Case 2, where a faster response is required, i.e. shorter settling times, the thruster has a higher demand, as can be seen in Figure 3.28. On the other hand, the performances have improved, as required in Case 2. The position of the satellite in this case can be seen in Figure 3.25 and Figure 3.26. The error response in Figure 3.27.

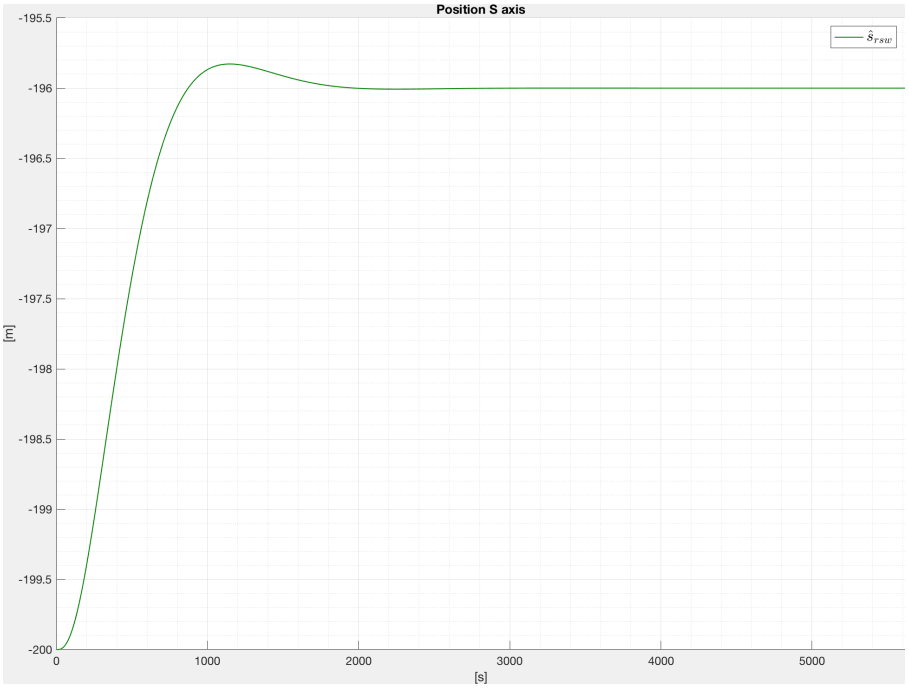


Figure 3.25: Case 2 — Position response in S axis

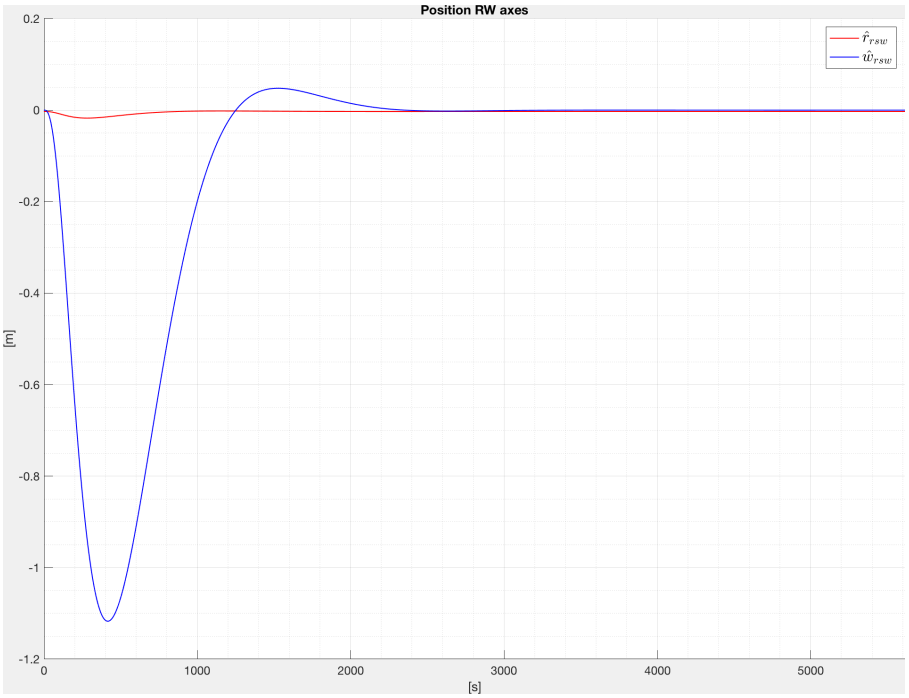


Figure 3.26: Case 2 — Position response in RW axes

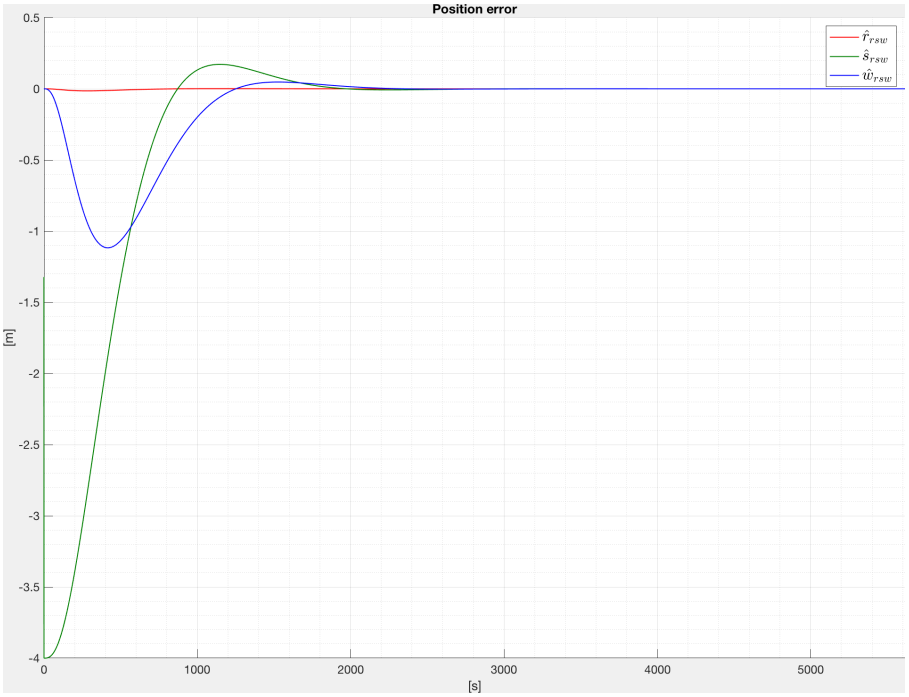


Figure 3.27: Case 2 — Error response

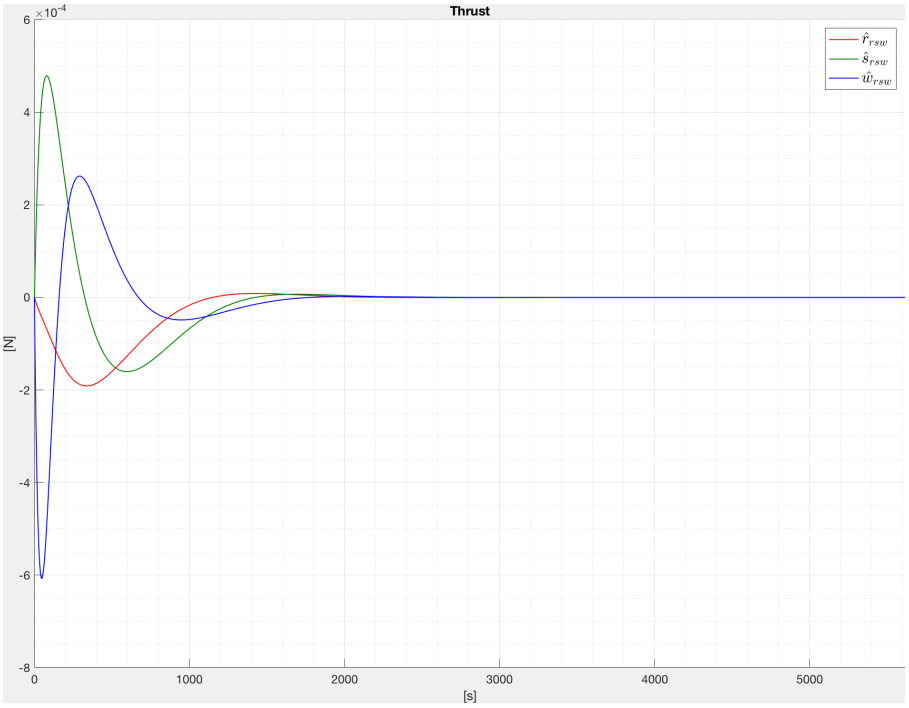


Figure 3.28: Case 2 — Thrust response

4 Simulations and results

In order to test the results of the control system obtained in §3.2, the plant has been substituted by a integrated DKE, with independent leader and follower satellite's DKE, coordinate system transformations, and input port for external thruster contributions. The complete simulation model is shown in Figure 4.1 and the integrated DKE in Figure 4.2.

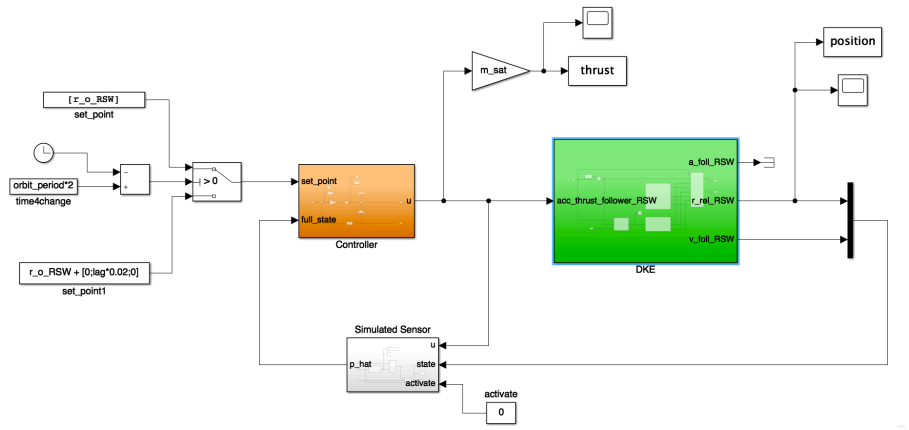


Figure 4.1: Complete simulation model

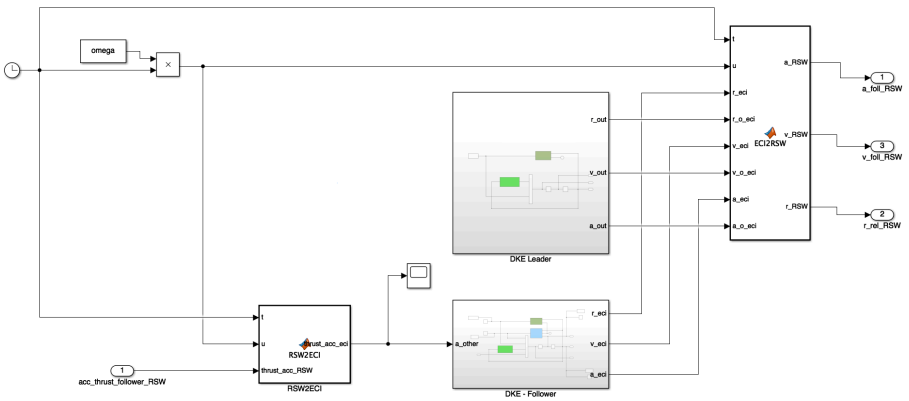


Figure 4.2: Integrated DKE used for the simulations

Before entering into test details, it would be interesting to see how the formation behaves when left uncontrolled, i.e. graph of the distance between satellites.

The model in Figure 4.3 has been created to measure the distance (norm of the vector) throughout two orbits, and the results can be seen in Figure 4.4. It is clear that a control system greatly improves the stability of the distance between leader and follower.

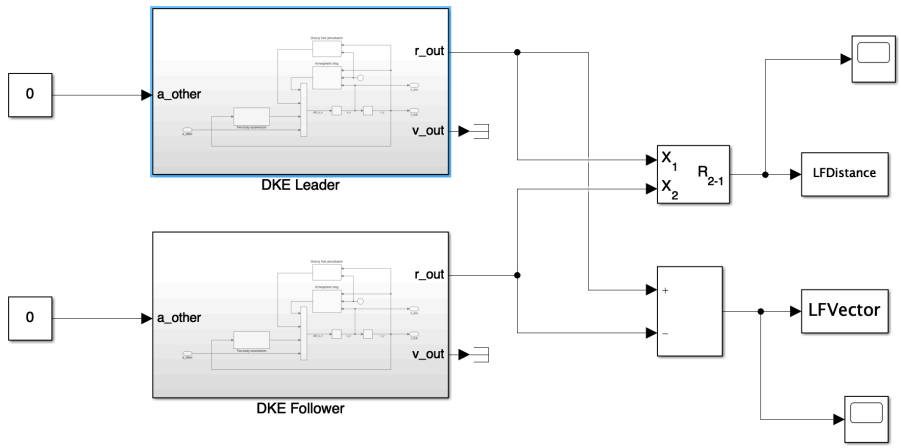


Figure 4.3: Model used to check the distance when the satellites are left uncontrolled

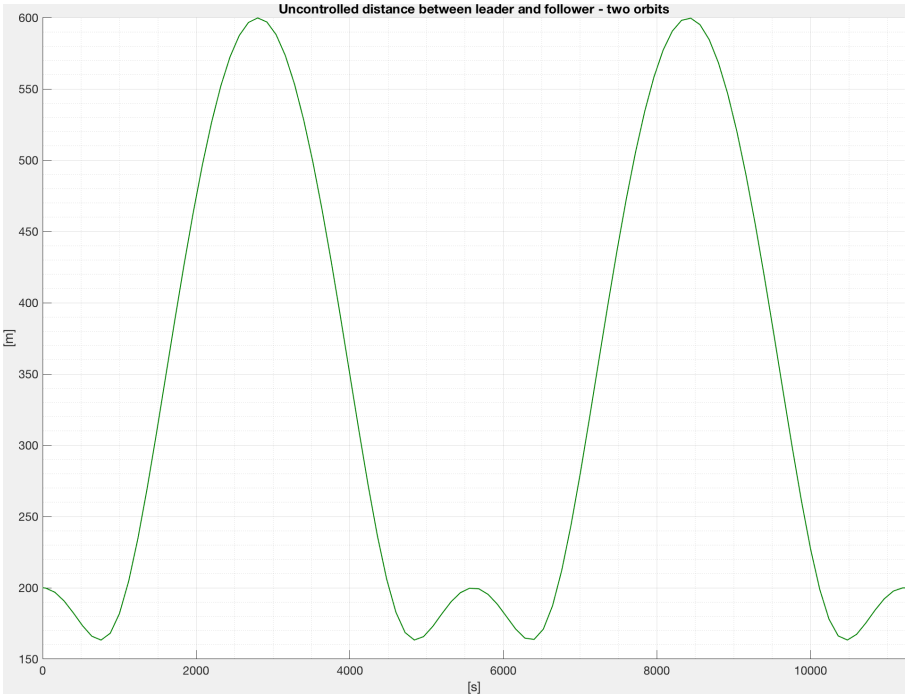


Figure 4.4: Uncontrolled distance between leader and follower satellites

4.1 Test cases

The cases of §3.3 are going to be simulated with the DKE instead of the plant in order to verify that their behavior is equivalent. There are some expected differences due to J2; e.g. reference tracking precision, perturbations, etc; however, the main characteristics of overshoot and settling times should be similar.

The two simulated cases are listed again for convenience:

1. Case 1 — Proposed nominal case:
   - $r(t < 2\lambda_{orbit}) = -200\,\text{m}\ \hat{s}_{rsw}$,

- $r(t \geq 2\lambda_{orbit}) = -196\,\text{m}\ \hat{s}_{rsw}$,
- $t_s = 2807\,\text{s} \approx \frac{\lambda_{orbit}}{2}$ and
- $\zeta = \sin(45) \approx 5\,\%_{\text{os}}$.

2. Case 2 — Alternative case:

- $r(t < 2\lambda_{orbit}) = -200\,\text{m}\ \hat{s}_{rsw}$,
- $r(t \geq 2\lambda_{orbit}) = -196\,\text{m}\ \hat{s}_{rsw}$,
- $t_s = 1403\,\text{s} \approx \frac{\lambda_{orbit}}{4}$ and
- $\zeta = \sin(45) \approx 5\,\%_{\text{os}}$.

Please note that with the plant it was possible to start the simulation before $t = 0$ and take advantage of this possibility to get a good steady-state at $t = 0$. In the case of the simulation with DKE this is not possible and therefore the times have been rearranged accordingly.

4.2 Test results

In the test results of the following sections, the simulation starts at $t = 0$, at $2\lambda_{orbit}$ there is an instantaneous change in the reference set point of $-2\,\%$ of the distance in the S axis, and it ends at $4\lambda_{orbit}$.

The startup transient is visible in the first minutes, this is due to the initial conditions of the different model elements, i.e. the initial states in some blocks; nevertheless, the system quickly recovers the nominal performance. The graphs are left as is, showing the complete simulation.

4.2.1 No sensor error

4.2.1.1 Case 1

Comparing the responses in Figure 3.21, Figure 3.22 and Figure 3.23 with those in Figure 4.5, Figure 4.6 and Figure 3.23, respectively; shows that the control system produces very similar overshoots and settling times, with both the plant or with the DKE.

Comparing thruster demands, of Figure 3.24 and Figure 4.8, it becomes apparent the importance of the J2 Zonal Harmonic contribution, not present in the plant. To compensate this contribution, the thruster has to follow this profile in order to maintain small position errors. On the other hand, the shape of the response to the reference point change is very similar in both cases.

One interesting observation from Figure 4.8 and Figure 4.12 is that there is a small drift on the R component that does is not present when controlling the plant, as can be seen in Figure 3.24 and Figure 3.28. It does not show either in the S and W axis of these graphs. In addition, the line shows a sinusoidal component with a period of about $\frac{\lambda_{orbit}}{2}$ in both simulation configurations.

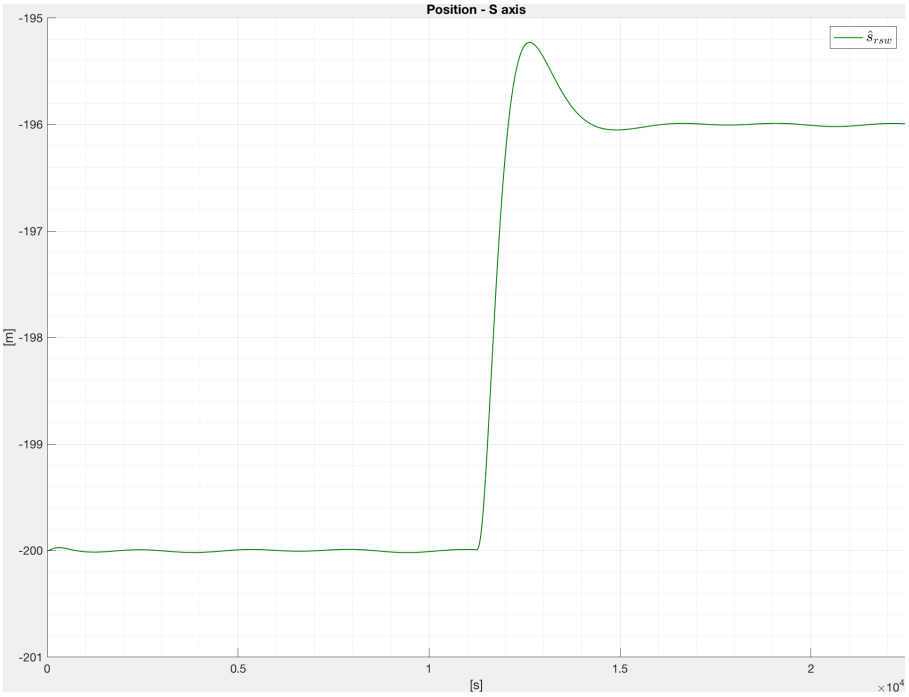


Figure 4.5: Case 1: Simulation without sensor error — Position in S axis

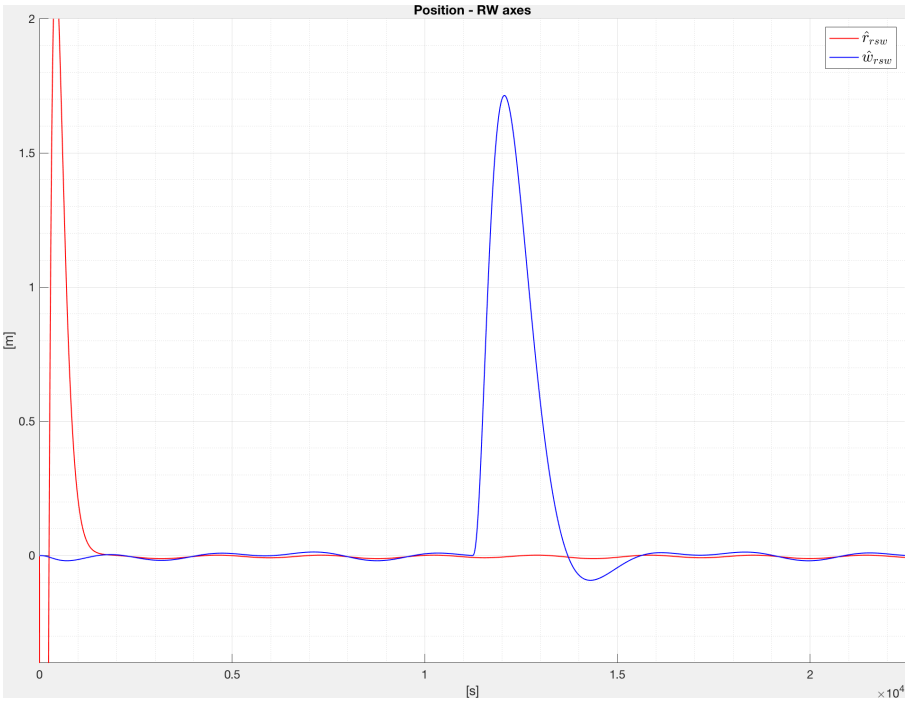


Figure 4.6: Case 1: Simulation without sensor error — Position in RW axes

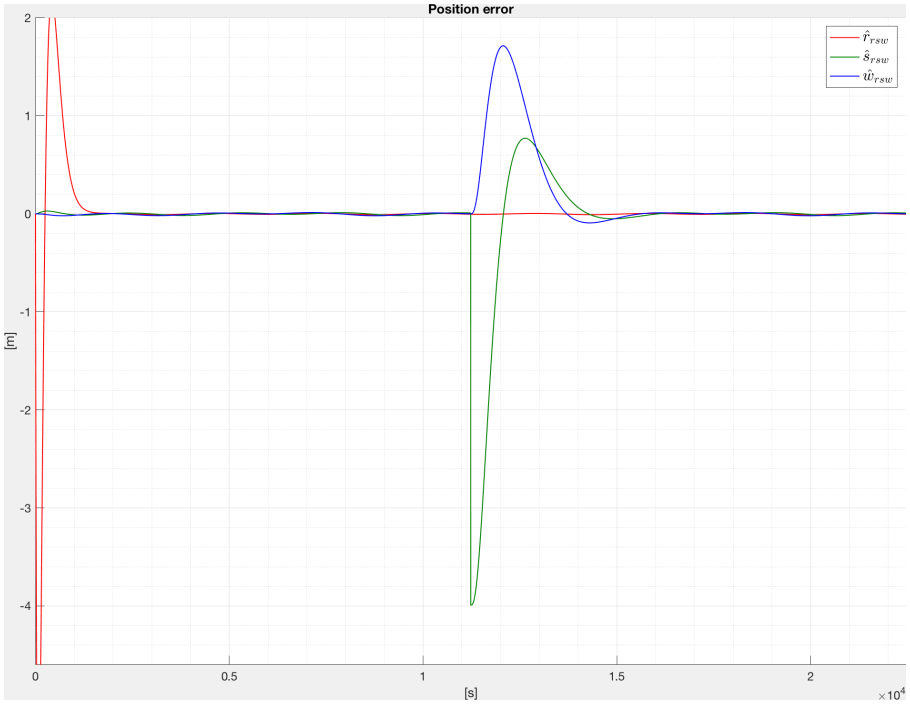


Figure 4.7: Case:1 Simulation without sensor error — Error response

This component is radial and collinear with the $\vec{\mathbf{r}}_{eci}$ vector and any positive acceleration tries to push the satellite to a higher orbit.

It would be difficult to assess this drift without performing simulations over a longer period of time. Nevertheless one potential root cause could be the simplified modeling of orbital motion and coordinate transformations. For example, in many equations it is assumed that the leader satellite has constant angular velocity and orbits uniformly around the sun, that the orbit precedes with uniform angular velocity, that coordinate system transformation only need to take into account IJK' precession and RSW rotation, etc. Another potential root cause could be the accumulation of numerical errors in the propagator. Although these circumstances could be perfectly valid for a preliminary dimensioning to model these kind of control systems, a more precise approach might be necessary in future activities.

4.2.1.2 Case 2

Comparing the responses in Figure 3.25, Figure 3.26 and Figure 3.27 with those in Figure 4.9, Figure 4.10 and Figure 3.27, respectively; shows that in this case the control also produces very similar responses, in terms of overshoot and settling time.

Comparing thrust graphs of Figure 3.24 and Figure 4.8 with those of Figure 3.28 and Figure 4.12, shows an important increment in the thruster demand.

It has been shown, that the desired maximum thrust can be obtained by tuning the settling time parameter.

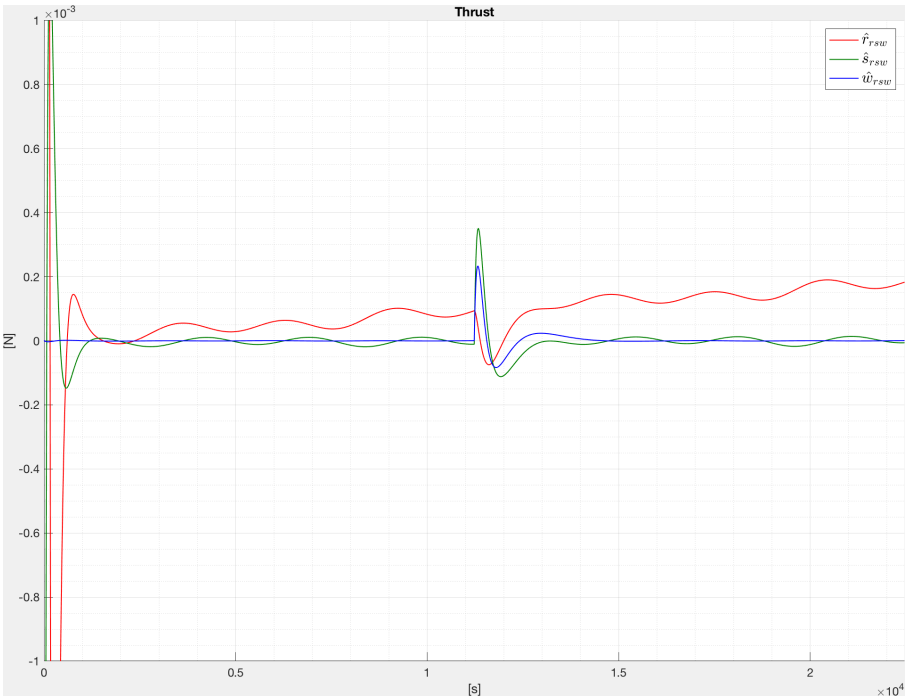


Figure 4.8: Case 1: Simulation without sensor error — Thrust demand

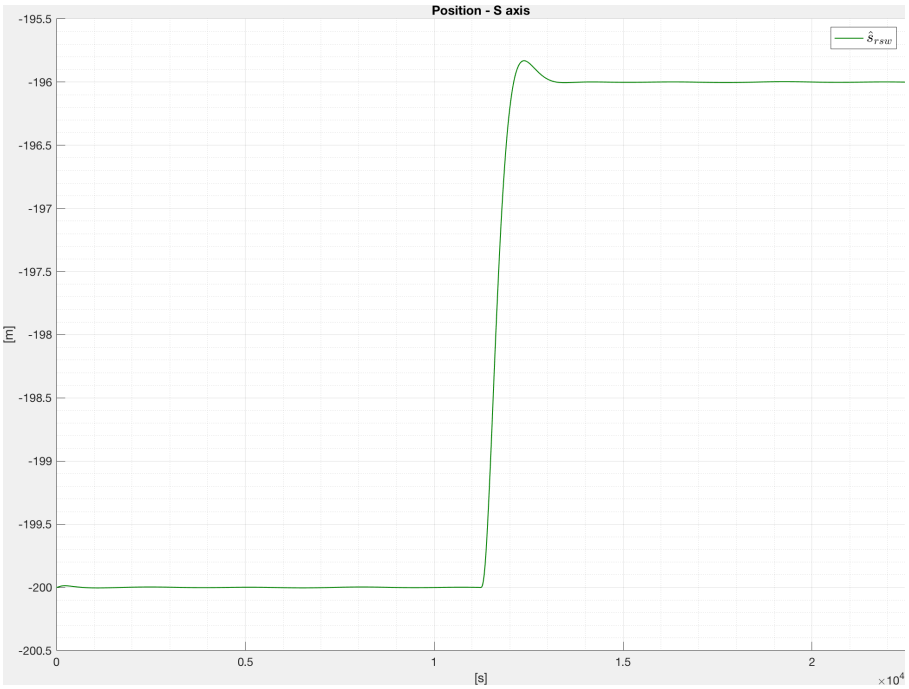


Figure 4.9: Case 2: Simulation without sensor error — Position in S axis

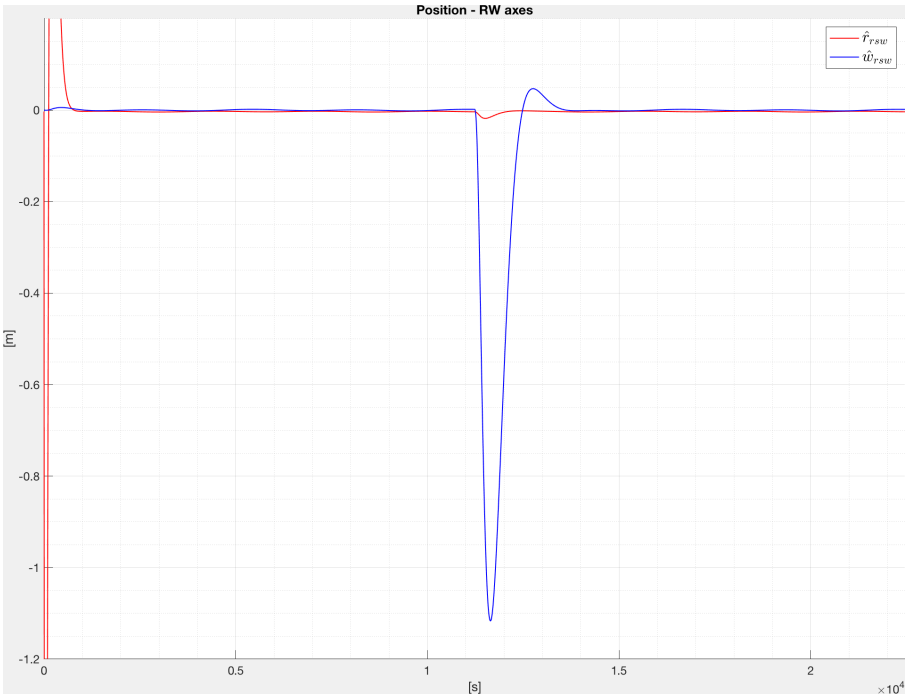


Figure 4.10: Case 2: Simulation without sensor error — Position in RW axes

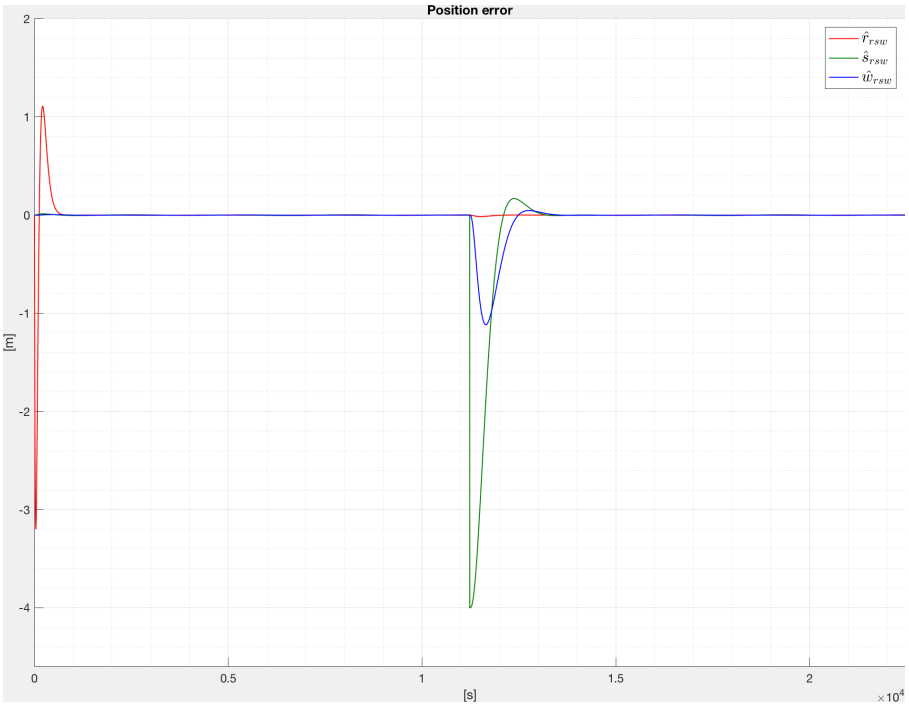


Figure 4.11: Case:2 Simulation without sensor error — Error response

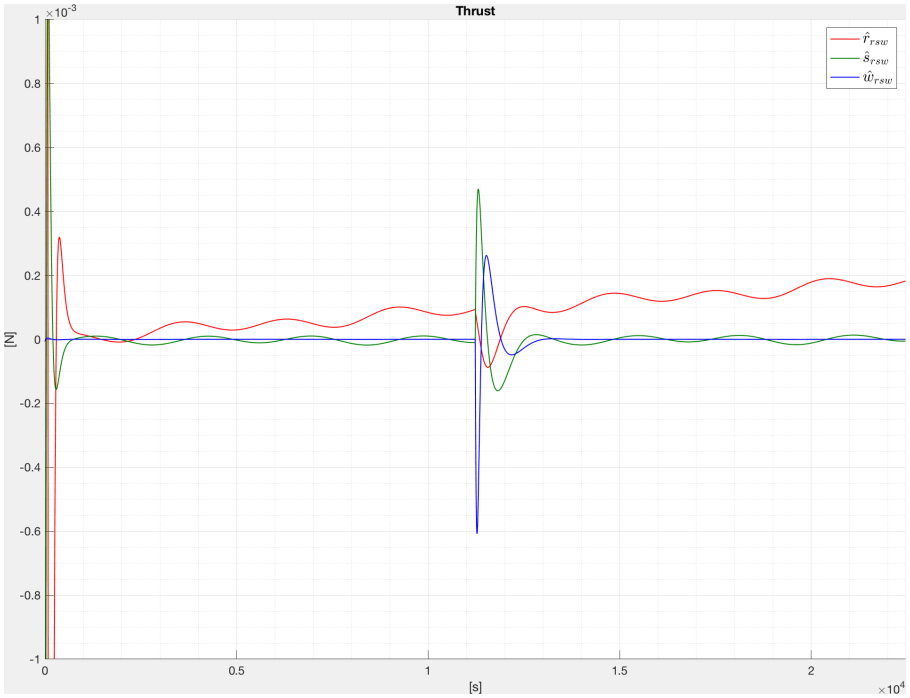


Figure 4.12: Case 2: Simulation without sensor error — Thrust demand

4.2.2 With sensor error

In order to compensate for sensor errors it is necessary to have a model of the error profile and noise, and then create the corresponding compensator, or adjust an existing one. This would require specific sensor models and, potentially, real hardware measurements of their performance. This selection would ideally come from a mission analysis and the corresponding trade-off. Although this activity was not considered in the present project, it would be interesting to see the performance of the control of §3.2 without any compensation for sensor noise.

This simulation will use the Case 1 and the error profile of Figure 4.13, Figure 4.14 and Figure 4.15. In these figures, the yellow graph corresponds to the position error with a normally distributed band-limited white noise. The magenta graph corresponds to the output of a Kalman filter that is fed to the control. Kalman filters require a specific tunning, however, in this case, a preliminary qualitative tuning has been performed.

As in the case of §4.2.1, the first minutes of simulation show the startup transient, quickly followed by the steady-state.

For these inputs, the actual position, as obtained from the DKE, is depicted in Figure 4.16 and Figure 4.17. The error obtained in this case is less than 1 m, which can also be seen in Figure 4.18.

Although the performance of the control system is still similar to the results described in §4.2.1, the degradation is evident. It would be necessary then, to include sensor error compensation.

Analyzing Figure 4.19, it seems that the control is reacting heavily and fast to sensor-error perturbations, this is due on how the controller was created, with specific settling times and

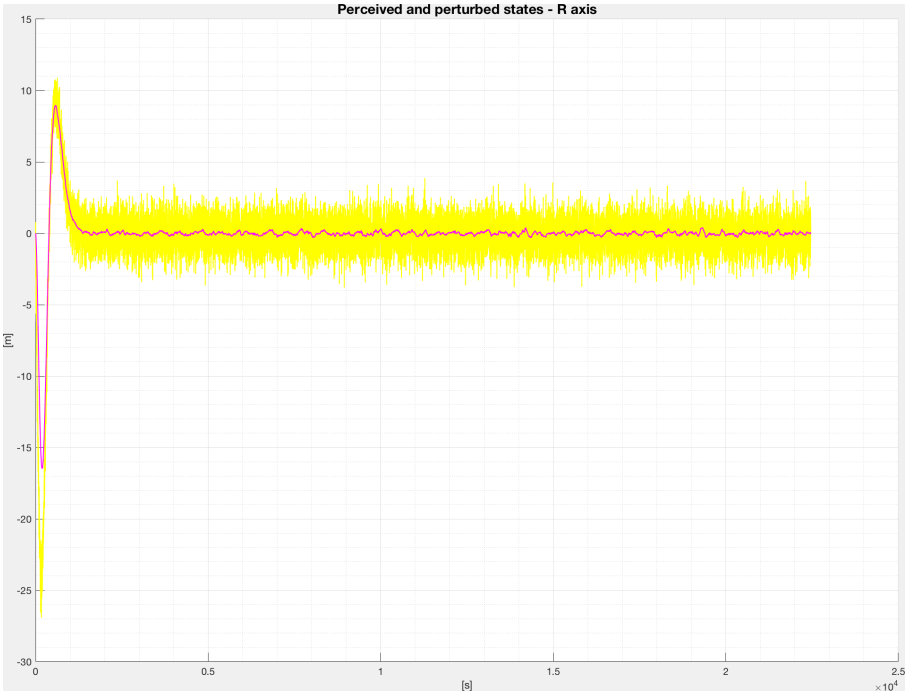


Figure 4.13: Case 2: Simulation with sensor error — Perturbed and perceived positions in R axis

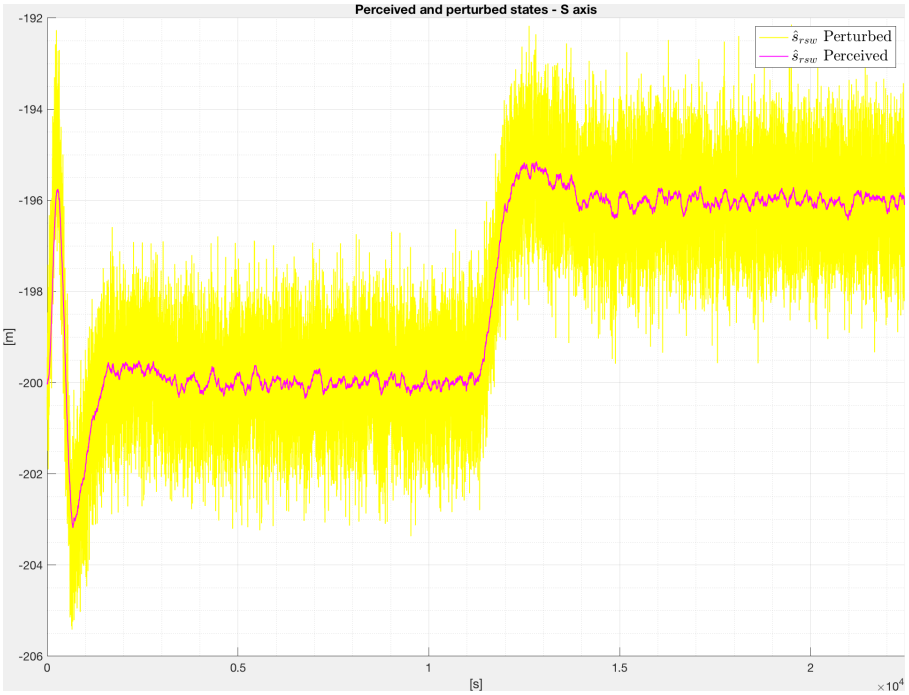


Figure 4.14: Case 2: Simulation with sensor error — Perturbed and perceived positions in S axis

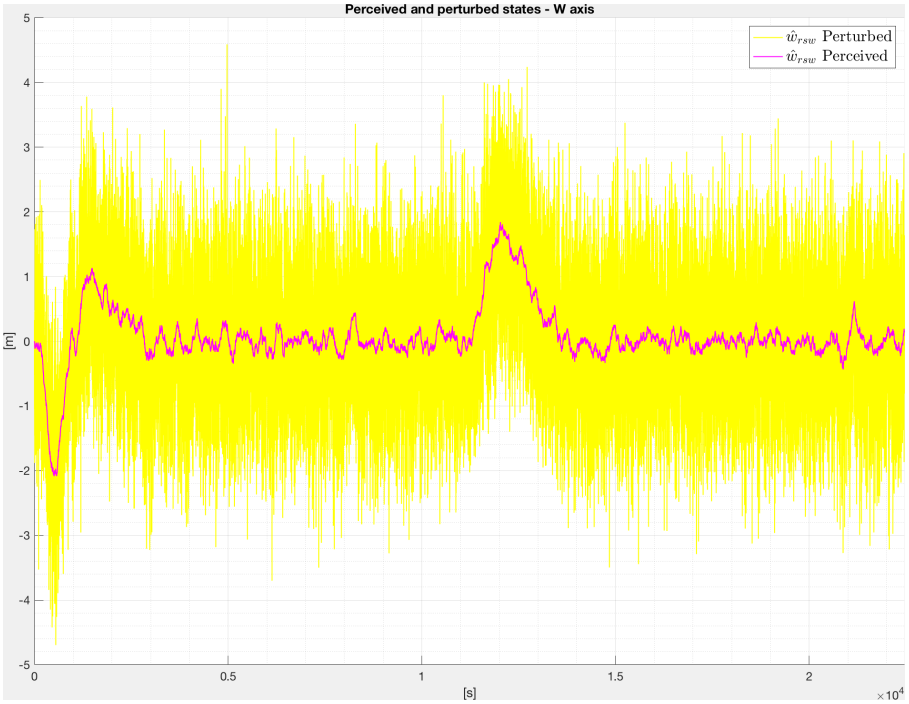


Figure 4.15: Case 2: Simulation with sensor error — Perturbed and perceived positions in W axis

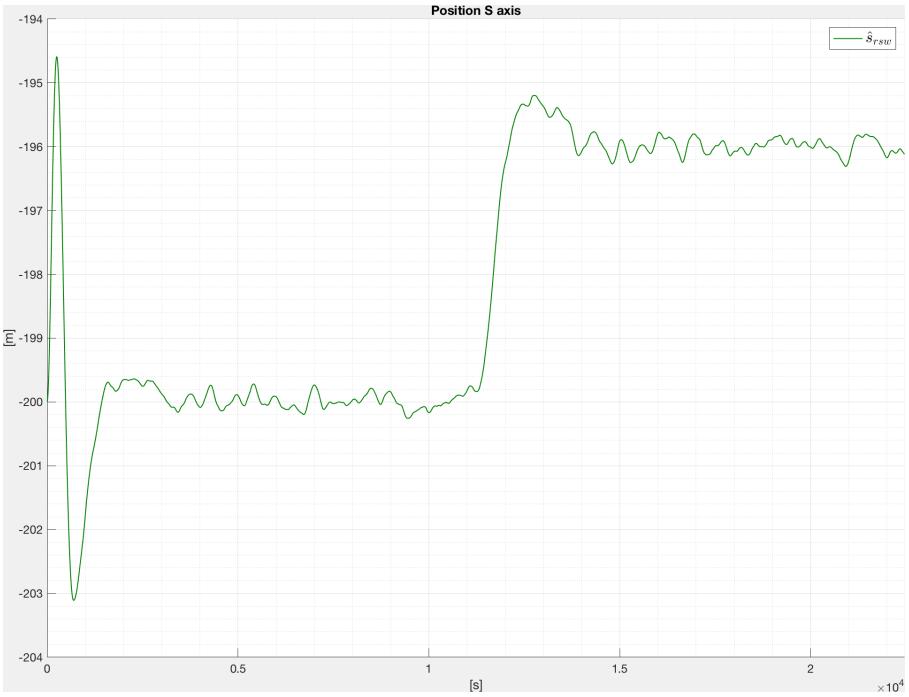


Figure 4.16: Case 2: Simulation with sensor error — Actual position in S axis

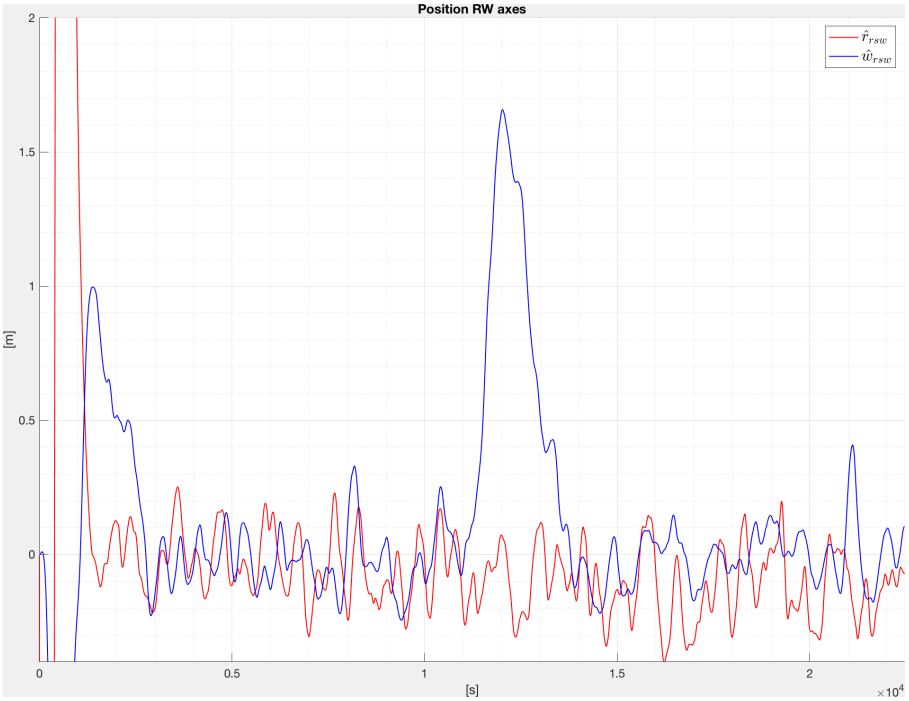


Figure 4.17: Case 2: Simulation with sensor error — Actual position in RW axis

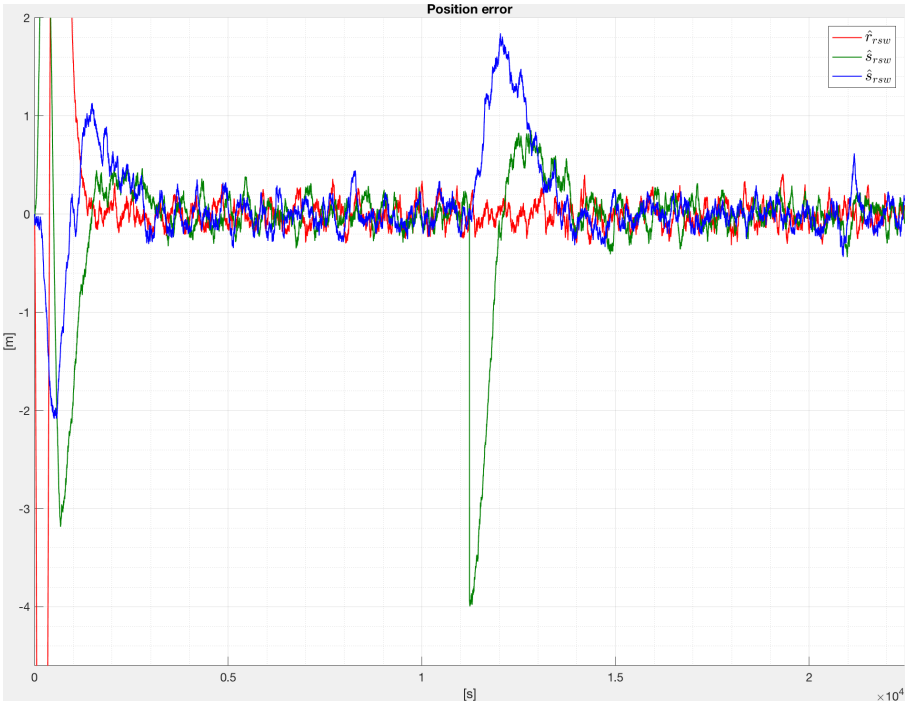


Figure 4.18: Case 2: Simulation with sensor error — Error

overshoot parameters using second order dominant poles. Tunning the Kalman filter to provide smoother responses would imply longer reactions that would need to be taken into account by the controller. Applying a specific filter, or extending the control system to compensate for this normally distributed white noise might be another option. Relaxing the settling time restriction would also improve the response when coupled with anyone of the aforementioned options. In any case, it would be necessary to have a profile of the sensor-error and noise profile in order to perform a good design.

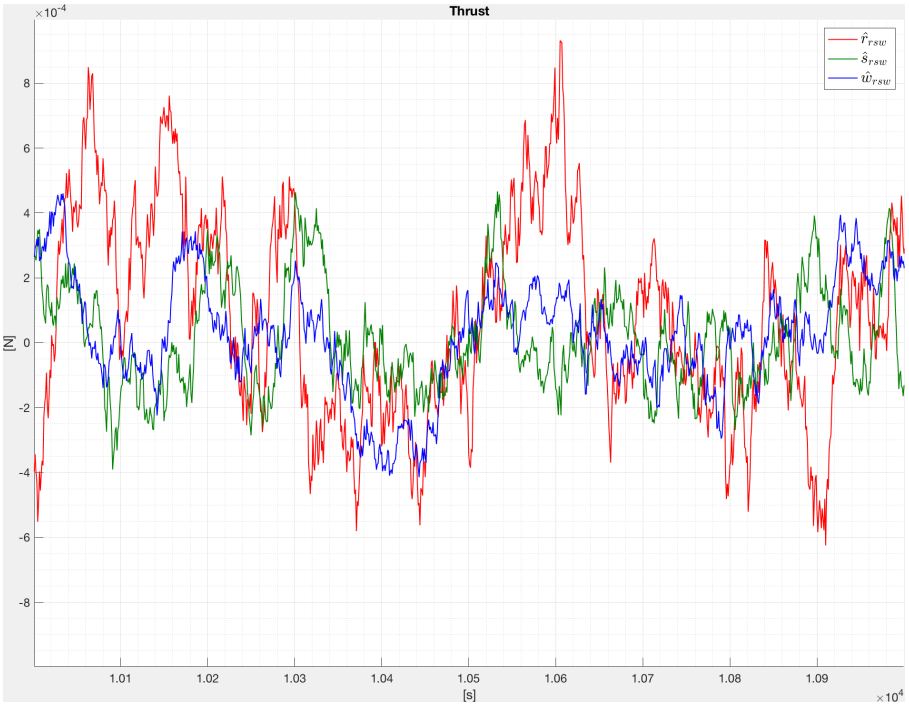


Figure 4.19: Case 2: Simulation with sensor error — Detail of 1000 s of thrust in steady-state

5 Results discussion and future work

From the results presented in the simulations of §4, it can be seen that the response obtained with the plant (§3.2) is very similar to the response obtained with the DKE simulations, and in both systems the control is able to achieve position errors under 10 cm. In addition, when performing formation resizing of −2 % in the S axis, the control system is able to regain steady-state in the prescribed settling time.

In the proposed cases, during formation resizing the thrust demands have been kept under 400 µN in each axis; nevertheless, a parametrized set of equations have been put in place to tune the overshoot and settling time in order to adjust thrust demand to potential mission requirements. The only exception is the simulation with sensor-error, in which the thrust demand raised due to an increase in the control activity. A future version of this control would need to include provisions to compensate for this sensor-errors.

It has been shown that the models created from the HCW equations can effectively be used for the analysis of mission scenarios and the implementation of a control system. In addition, a set of simulation models and DKEs have been created that can support future inquiries on this kind of formation flying scenarios.

Finally, due to the low thrust provided by an electric propulsion system, long orbit control maneuvers are required. Therefore, mission design is highly affected by long-term attitude and power constraints.

In conclusion, a CubeSat formation flying with electric propulsion thrusters seems to be realizable in scenarios similar to the ones presented in this project.

5.0.1 Future work

From a system level feasibility point of view, it is advised that future works include a simplified electric power system model that considers power source and energy storage components. This model could be coupled with the orbital simulator developed in this project in order to determine the power availability required to actuate the electric propulsion thrusters during the time and within the required thrust control ranges.

In this project, the attitude control of the satellite has not been considered. This is a complex, but fundamental, problem that requires in-depth analyses for each mission. One of the first activities that should be performed is to translate the thruster requirements given in RSW axes

into a set of thrust components that can be actually exercised by an attitude control system, e.g. by means of reaction wheels. This problem can be proposed for future works.

Regarding sensor error compensation, it was clear in §4.2.2 that although the control system was able to maintain the position error within 1 m, the performance was degraded. A proposed future work would be to extend the current control implementation to compensate for the sensor error, fine tune the Kalman filter, relax settling time constraints or introduce a specific block for sensor error compensation.

Regarding the small drift observed in Figure 4.8 and Figure 4.12, it is proposed to assess the potential root causes presented in §4.2.1, by revising the implemented orbital dynamics and the contributions of the J2 term, perform longer simulations, and improve the DKE.

Finally, this project was a first approach to the problem of CubeSat formation flying for electric propulsion devices, focusing on the potential demands that this type of missions would impose on such devices. This analysis can be extended to include better models, more precision and accuracy, additional actuators and sensors, better control, an attitude control system, navigation, etc.

A Glossary of symbols

A: It is the cross sectional area perpendicular to the motion.

A: Standard state-variable form, A matrix.

a**:** Semi-major axis.

α**:** Generic angle.

$\vec{\mathbf{a}}_{eci}$**:** Acceleration in ECI frame.

$\vec{\mathbf{a}}_{ijk'}$**:** Acceleration in IJK' frame.

$\vec{\mathbf{a}}_{t_{eci}}$**:** Thruster acceleration in ECI frame.

$\vec{\mathbf{a}}_{t_{rsw}}$**:** Thruster acceleration in ECI frame.

a_x**:** X accelerations due to external forces in HCW formulation.

a_y**:** Y accelerations due to external forces in HCW formulation.

a_z**:** Z accelerations due to external forces in HCW formulation.

B: Standard state-variable form, B matrix.

c_D**:** It is the coefficient of drag.

deg**:** Angular degrees.

e**:** Eccentricity.

$\vec{\mathbf{e}}$**:** Tracking error.

eig: Eigenvalue operator.

F: The system matrix.

G**:** Universal gravitational constant.

G: The input matrix.

H: The output matrix.

$\vec{\mathbf{h}}_{eci}$: Angular momentum.

i: Inclination.

$\hat{i}$: Unitary vector. ECI axis points towards the vernal equinox of year 2000.

$\hat{j}$: Unitary vector. ECI axis together with $\hat{i}$ form a plane contained in the equatorial plane.

$\hat{i}'$: Intermediate I axis for RSW transformation.

J: The direct transmission matrix.

$\hat{j}'$: Intermediate J axis for RSW transformation.

J2: Earth's J2 Zonal Harmonic.

K: Control law gain.

$\hat{k}$: Unitary vector. ECI axis points toward the north pole in order to form an orthonormal frame.

$\hat{k}'$: Intermediate K axis for RSW transformation.

km: Kilometer.

$\mathscr{L}$: Laplace transform.

λ_{orbit}: Period of the orbit.

M: Transformation matrix.

m: Meter.

$m_{\oplus}$: Mass of Earth.

m_{sat}: Mass of the satellite.

μ: Gravitational parameter.

$\vec{\mu}$: Input vector in Error-Space.

μN: Micro Newton.

mN: Milli Newton.

$\vec{\mathbf{n}}$: Ascending node.

N: Newton.

ν: True anomaly.

Ω: Right ascension of the ascending node.

ω: In Keplerian elements it is the argument of the perigee; in HCW formulation is the leader satellite's orbital angular velocity.

ω_d: Imaginary part of the pole (and damped frequency).

ω_n: Natural frequency.

ω_{sat}: Is the angular velocity of the satellite around Earth.

$\vec{\mathbf{p}}$: State vector in State Space.

π: Pi number.

$\vec{\mathbf{q}}$: Output vector in State-Space.

$\vec{\mathbf{r}}$: Reference input in Error-Space formulation.

$\hat{r}$: Unitary vector. R axis in RSW frame.

ρ: It is the atmospheric density.

rank: Rank operator.

$\vec{\mathbf{r}}_{eci}$: Position in ECI frame.

$\vec{\mathbf{r}}_{ijk'}$: Position in IJK' frame.

$\vec{\mathbf{r}}_{pqw}$: Position in PQW frame.

$\mathbf{ROT}_1(\alpha)$: First axis elemental rotation.

$\mathbf{ROT}_2(\alpha)$: Second axis elemental rotation.

$\mathbf{ROT}_3(\alpha)$: Third axis elemental rotation.

s: Seconds; also the Laplace complex variable.

σ: Real part of the pole.

$\hat{s}$: Unitary vector. S axis in RSW frame.

T: Transfer function matrix.

t_s: Settling time.

u: Argument of latitude.

$\vec{\mathbf{u}}$: Input vector in State-Space.

$\vec{\mathbf{v}}_{eci}$: Velocity in ECI frame.

$\vec{\mathbf{v}}_{ijk'}$: Velocity in IJK' frame.

$\vec{\mathbf{v}}_{pqw}$: Velocity in PQW frame.

$\vec{\mathbf{v}}_{rel}$: The velocity of the satellite relative to the atmosphere.

W: Watt.

$\hat{w}$: Unitary vector. W axis in RSW frame.

$\vec{\xi}$: Error-Space State Vector.

$\vec{\mathbf{z}}$: Standard state-variable.

ζ: Damping ratio.

B Glossary of acronyms

COTS Commercial off the shelf.

DKE Dynamics, kinetics and environment.

ECI Earth Centered Inertial.

ESA European Space Agency.

FF Formation flying.

HCW Hill-Clohessy-Wiltshire equations.

IJK' Intermediate reference frame for transformation from ECI to RSW.

IJKP Matlab denomination for IJK', as the apostrophe cannot be used.

LEO Low Earth Orbit.

PC Personal computer.

PD Proportional-Differential.

PID Proportional-Integral-Differential.

PQW Perifocal coordinate frame.

RSW Satellite reference frame.

U CubeSat size unit.

C Annex — List of Matlab™ and Simulink™ files

The following Matlab™ and Simulink™ files are attached to this project and correspond to the models and scripts used for the development.

`HCW.mlx`
`HCW_ss_analysis.mlx`
`SS_plots.m`
`SS_satellite.slx`
`SS_tune_errorstate.slx`
`const_load.m`
`coordinate_transform.mlx`
`orbit_classical.slx`
`orbit_dke.slx`
`orbit_dke_plots.m`
`uncontrolled_satellites.slx`
`uncontrolled_satellites_plots.m`

It is necessary to excecute first the file `const_load.m` before executing any simulation as it loads all the required variables. The rest of the files have been explained in this report in the corresponding sections. Plotting helper scripts are also provided for convenience.

Bibliography

Angulo Jerez, Manuel, Segundo Esteban San Román, José María Girón Sierra, and Óscar I. Rodríguez Polo. "Control de Formaciones en Vuelo de Satélites de Bajo Coste." Creative Commons Attribution CC-BY-NC 3.0 license, 2018. https://creativecommons.org/licenses/by-nc/3.0/.

Bandyopadhyay, Saptarshi, Rebecca Foust, Giri P. Subramanian, Soon-Jo Chung, and Fred Y. Hadaegh. "Review of Formation Flying and Constellation Missions Using Nanosatellites." *Journal of Spacecraft and Rockets* 53, no. 3 (2016): 567–578. doi:10.2514/1.a33291.

California Polytechnic State University. *6U CubeSat Design Specification*. Technical report. California Polytechnic State University, April 20, 2016.

Clohessy, W. H., and R. S. Wiltshire. "Terminal Guidance System for Satellite Rendezvous." *Journal of the Aerospace Sciences* 27: 653-674 (1960).

Edlerman, Eviatar, and Igal Kronhaus. "Analysis of Nanosatellite Formation Establishment and Maintenance Using Electric Propulsion." *Journal of Spacecraft and Rockets* 54, no. 3 (May 2017): 731–742. ISSN: 0022-4650. doi:10.2514/1.a33632. https://doi.org/10.2514/1.A33632.

Ferrario, Alessandro, and Beatrice Furlan. "CubeSat formation flying mission as Wi-Fi data transmission and GPS based relative navigation technology demonstrator." Master's thesis, Politecnico di Milano, 2011.

Franklin, Gene F., J. David Powell, and Abbas Emami-Naeini. *Feedback Control of Dynamic Systems, 4th Edition*. Prentice Hall, 2002. ISBN: 0130323934.

Hill, George W. "Researches in Lunar Theory." *American Journal of Mathematics* 1: 5-26 (1878).

Kristiansen, Raymond, and Per Johan Nicklasson. "Spacecraft formation flying: A review and new results on state feedback control." *Acta Astronautica* 65, nos. 11-12 (2009): 1537–1552. doi:10.1016/j.actaastro.2009.04.014.

Persson, Staffan, Simone D'Amico, and Jon Harr. "Flight Results from PRISMA Formation Flying and Rendezvous Demonstration Mission." *61st International Astronautical Congress 2010, IAC 2010*, 2010.

Peterson, E. H., G. Fotopoulos, and R. E. Zee. "A Feasibility Assessment for Low-Cost InSAR Formation-Flying Microsatellites." *IEEE Transactions on Geoscience and Remote Sensing* 47, no. 8 (2009): 2847–2858. doi:10.1109/tgrs.2009.2017521.

Planetary Systems Corporation. *Payload Specification for 3U, 6U, 12U and 27U*. Technical report. Planetary Systems Corporation, July 21, 2014.

The MathWorks, Inc. *Aerospace Blockset User's Guide R2018a*. Natick, Massachusetts, 2018.

———. *Aerospace Toolbox User's Guide R2018a*. Natick, Massachusetts, 2018.

———. *Control System Toolbox Reference R2018a*. Natick, Massachusetts, 2018.

———. *MATLAB Function Reference R2018a*. Natick, Massachusetts: The MathWorks Inc., 2018.

———. *Simulink Reference 2018a*. Natick, Massachusetts: The MathWorks Inc., 2018.

Vallado, David A. *Fundamentals of Astrodynamics and Applications, 4th ed. (Space Technology Library)*. Microcosm Press, 2013. ISBN: 9781881883180.

Wertz, J. R., and W. J. Larson. *Space Mission Analysis and Design, 3rd edition (Space Technology Library, Vol. 8)*. Microcosm, 1999. ISBN: 1881883108.